学位論文

Evolution of the Lower Crust: Evidence from Petrology and Structural Geology of the Kohistan Arc, NW Himalayas

北西ヒマラヤ、コヒスタン島弧の岩石学・構造地質学と下部地殻の進化

平成9年12月 博士(理学)申請
東京大学大学院理学系研究科
地質学専攻

井 岡 聡

学 位 論 文

Evolution of the Lower Crust: Evidence from Petrology and Structural Geology of the Kohistan Arc, NW Himalayas

北西ヒマラヤ、コヒスタン島弧の
岩石学・構造地質学と下部地殻の進化

平成９年１２月博士（理学）申請

東京大学大学院理学系研究科
地質学専攻
芳野　極

Abstract

The lower crust defined as a layer between the Conrad and Mohoroviç discntinuities is significant constituent of the crust. The Kohistan arc, northern Pakistan, represents a section of lower crust of the Early Cretaceous island arc. In the present study, the lower crust rocks of the Kohistan arc were investigated based on both metamorphic petrology and structural geology to understand processes of formation of the mafic lower crust, fluid-rock interaction in the high temperature metamorphism and exhumation mechanism of high pressure rocks. The lower crust rocks consist of mainly metabasic rocks such as pyroxene granulites, garnet granulites and amphibolites derived from gabbronorite. Tectonic events of the lower crust in the Kohistan arc in the early Cretaceous ages can be divided into three major events: (1) intrusions of the basaltic to intermediate arc-derived magma; (2) subsequent formation of the pyroxene and garnet granulites under medium to high pressure granulite facies metamorphism; and (3) hydration of the granulites. Peak *P-T* conditions calculated based on Al zoning in clinopyroxene and plagioclase are 0.8-1.2 GPa at around 800 °C. Estimated prograde *P-T* paths represent a crustal thickening process suggesting loading above the lower crust. The crustal thickening in the lower crust of the Kohistan arc was attributed to the large scale magma intrusion at the middle crustal depth. Garnet granulites develop within the pyroxene granulites overprinted the pre-existing pyroxene granulites by consumption of hornblende, orthopyroxene and calcic plagioclase. Vein-like occurrence of the garnet reaction zone is caused by channelized infiltration of CO_2-rich fluid with low water activity. Infiltration of fluid involved high a_{CO_2} and sulafate leads to occasionally form the scapolite with high sulfate content in the Kohistan granulites. Following the crustal thickening and formation of the garnet granulite, the lower crustal sequence of the Kohistan arc underwent uplift accompanied by development of ductile shear zones and regional amphibolitization during two collisional events. The regional gneissose deformation with shear direction of top to the northwest facilitated the uplift of the high pressure rocks in the extensional field during the back-arc collision. The lower crust of the Kohistan arc terminated the exhumation before the main Himalayan collision.

Contents

Chapter I

General Introduction

The lower crust plays important role such as crustal evolution, magmatic underplating, fluid circulation, fluid-rock interaction, and material recycling under high temperature condition. Comprehensive understanding of growth processes, chemical compositions, ages and physical properties of the lower crust still remains not to be attained. Important constraints on the nature of the lower crust have been provided by many authors on the basis of geological, petrological and geochemical investigations of granulite terranes in the world. Fountain & Salisbury (1981) identified five terranes (Ivrea zone, Fraser Range, Musgrave Range, Pikweitonei domain, Kasila series), and they compared these exposed crustal sections to study the broader views of the composition, structure and evolution of the lower crust. Investigation of several exposed lower crustal section confirmed the physical continuity of high-grade rocks near or at the surface with deeper crustal levels. Geophysical data collected over the Arunta block in central Australia (Goleby *et al.*, 1989), Doubtful Sound in New Zealand (Oliver & Coggen, 1976; Oliver, 1990), Ivrea zone in northern Italy (Schmid & Wood, 1976; Fountain, 1976) and Kapskasing uplift in Ontario, Canada (Percival & McGrath, 1986; Percival *et al.*, 1989), made possible to speculate that these regions exposed the lower portions of the continental crust. Based on the compilation of these lower crustal sections, Percival *et al.* (1992) suggested that the crustal composition change generally from felsic at high structural level to intermediate, mafic or anorthositic at deep structural level. On the other hand, Griffin & O'Reilly (1987) emphasized the predominance of mafic granulites with subordinate amounts of felsic metaigneous rocks and rare metasediments. According to compilation of granulite data of Rudnick & Presper (1990), Archean granulite terranes tend to be dominated by

andesitic compositions, post-Archean granulite terranes have a wide range in more mafic compositions, whereas granulite xenoliths are distinctly dominated by mafic lithologies. Differences between the intermediate compositions of the exposed lower crustal section and the mafic composition of the xenolith suggest that most of exposed lower crustal section does not always represent the lowermost crust. Especially exhumation of high pressure granulites such as garnet granulites showing the lowermost crust are rare, and therefore it is difficult to construct the overall crustal columns. Since study of the lower crustal xenolith is not enough to clarify the spatial distribution of lithology and structure, it should be firstly required to research the lower crustal section composed of mostly mafic composition in the world. The Kohistan arc is one of the most excellent terranes to study the lower crust with dominantly mafic composition. Geological setting of the Kohistan arc will be introduced in Chapter II, and field relations in the Kohistan arc will be described in Chapter III.

The author consider that the situation of island arc is one of the most significant sites to the formation of the continental crust. If an island arc stands on oceanic crust, it generates formation of the thick crust by subduction-related magmatism. If this island arc subsequently collides with a continent, it can add material in the form of exotic terranes. Magmatic underplating of mantle-derived basaltic magmas contributes large volumes of material to the continental crust in different tectonic settings and triggers metamorphism, melting and magmatic activity in the crust (Kay *et al.*, 1992). Large exposures of possibly underplated rocks of basaltic composition are rare at the surface. The Kohistan arc is exotic terrane between the Asian and Indian continents and subduction-related Cretaceous magmatic arc with calc-alkaline affinity (*e.g.* Coward *et al.*, 1982; 1986) (Fig. 1-1). Because the lower crust of the Kohistan arc commonly has mafic composition derived from gabbroic magma (Khan *et al.*, 1993), magmatic underplating should be considered as a crust formation mechanism. During the period of subduction-related magmatism, the underplated materials at middle to deep crustal level should subsequently undergo

metamorphism under high-T conditions corresponding to the amphibolite and the granulite facies. Hence many high-grade metamorphic rocks derived from gabbroic protolith in the lower crust should preserve many information of the metamorphism after cooling of magmatic intrusion. Metamorphic P-T paths of the rocks clearly provide constraints about process of crustal evolution. In Chapter IV, the metamorphic P-T paths of the lower crust of the Kohistan arc were inferred from Al-zoning in clinopyroxene and plagioclase.

Fluid transport in crustal rocks is a fundamental process controlling the geochemical evolution of the continental crust (Ferry, 1980; Etheridge *et al.*, 1983; Newton, 1989). Deep crustal fluids probably mostly comprise complex mixtures of various components (the most important of which are H_2O and CO_2 but which also include other species such as CH_4, N_2, SO_2, and rare gases) and also various dissolved species. Some of these fluids are intensively interact with silicate minerals at high pressures and temperatures, and can promote partial melting. Supercritical fluids with very low viscosity also have high mobility and are theoretically able to transport dissolved components over large distances. Therefore, they are capable of altering the chemical and isotopic composition of large portions of the crust. The fluid compositions, temperatures and pressures completely control the stability of mineral assemblages, mineral solubilities and degassing reaction. Understanding the behavior of fluids in the lower crust is a first-order geological problem and necessarily involves a more comprehensive understanding of the various physical and chemical processes in the lower crust. In the high grade gneiss terranes, fluid inclusion studies (e.g. Touret, 1971; Hansen *et al.*, 1984; Hollister, 1988) and thermodynamic calculations (e.g. Lamb & Valley, 1984, 1985, 1988; Newton, 1985, 1989; Edwards & Essene, 1988; Chacko *et al.*, 1988; Moecher & Essene, 1991) suggest that fluid composition in many granulite terranes world wide is generally CO_2-rich. Newton *et al.* (1980) proposed a model of large-scale CO_2 infiltration into the lower crust. However, Lamb *et al.* (1987) pointed out that in some cases CO_2-rich fluids were

introduced into these rocks long after the metamorphic peak. In the Kohistan arc, fluid species such as CO_2 and H_2O in the case play important roles such as amphibolite overprinting, development of vein-related reaction zones and presence of scapolite as CO_2 reservoir. In particular, variable occurrence of the garnet in the Kohistan granulites seems to be intensively controlled by fluid distribution in the lower crust. In Chapter V, fluid transport and composition of the lower crust will be discussed based on description of distribution of the vein, vein-related reaction zone and fluid-mineral equilibria.

Exhumation mechanism of the exposed lower crustal sections is also controversial. Some granulite terranes appear to be a single cycle from metamorphism to exhumation through the same tectonic process (Hollister & Crawford, 1986). Other granulite terranes have had to require for the exhumation process due to later tectonic episodes unrelated to formation of the granulite terrane (Thompson & England, 1984; Harley, 1985; Ellis, 1987; Bohlen, 1987). Occurrence of the exposed lower crust commonly represents detached fragments in the high-grade gneiss terrane. Exhumation of high pressure granulites, that is garnet granulites in the Kohistan arc, provides the chance of investigation for not only development of lowermost crust but also the exhumation mechanism. The exhumation mechanism of the high pressure granulite terrane should be considered in unusually tectonic environment. The retrogressive deformation structure is a clue to elucidate the exhumation mechanism of the high grade terranes. In the Kohistan arc, localized retrograde shear zones with variable mineral assemblage widely develops together with extremely hydration in the granulite terrane. In Chapter VI, the exhumation history of the lower crust of the Kohistan arc will be clarified based on deformation style, kinematics and mineral assemblage forming the variable types of foliation.

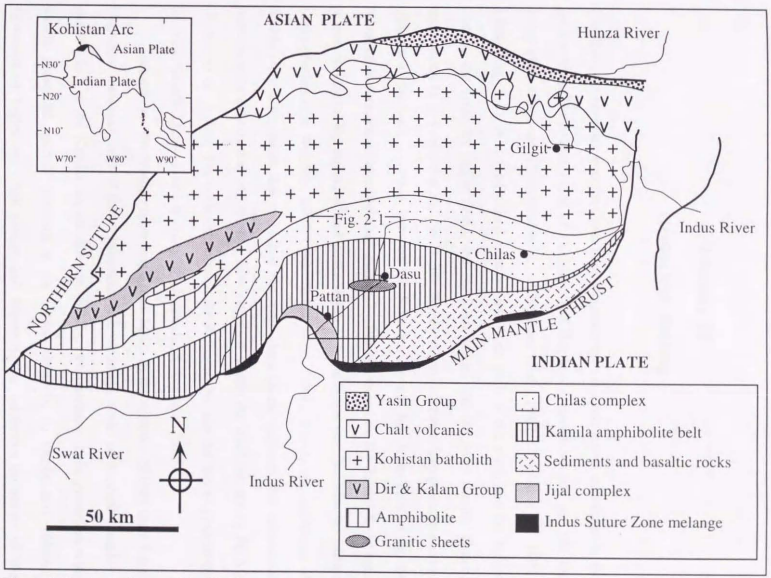

Fig. 1-1. Geological map of the Kohistan arc (modified from Treloar *et al.*, 1990; Yamamoto, 1993).
Inset: Locality of the Kohistan arc.

Chapter II

Geological Setting

The Kohistan complex was the Cretaceous magmatic intra-oceanic island arc located in the northwestern Himalayan range of Pakistan, and displays a crustal section (*c.* 200 km wide) of an island arc (Tahirkheli *et al.*, 1979; Bard *et al.*, 1980; Coward *et al.*, 1982, 1986) (Fig. 1-1). It is sandwiched between the Asian plate to the north and the Indian plate to the south by major faults, the Northern Suture and the Main Mantle Thrust, respectively (*e. g.* Coward *et al.*, 1982). The Kohistan arc underwent two collision events. Closure of the back arc basin between the Kohistan arc and the Asian plate along the Northern Suture was inferred to occur during 75-102 Ma, based on Rb-Sr and K-Ar ages of syn-collisional leucogranites and post collisional basic dykes intruded into the suture zones (Petterson & Windley. 1985; 1992; Treloar *et al.*, 1989). A K-Ar muscovite age of 66 Ma from a pegmatite that cross-cuts the main shear fabric indicates that substantial post-shearing exhumation and cooling have occurred within the Kohistan arc by 60 Ma (Treloar *et al.*, 1989). The collision between the Kohistan arc and the Indian plate along the Main Mantle Thrust started at about 50 Ma (Patriat & Achache, 1985).

Toward the structurally higher level, rock facies of the complex change from basal blueschist melanges, high-*P* garnet granulites and ultramafic rocks of the Jijal complex, amphibolites of the Kamila amphibolite belt (KAB), two-pyroxene mafic granulites with locally preserved igneous layering in the Chilas complex, to clastic and volcanic sediments of Jaglot and Chalt groups and Albian-Aptian calcareous sediments of the Yasin group from south to north (e.g. Coward *et al.*, 1986; Treloar *et al.*, 1996) (Fig. 2-1). Many igneous rock masses of tonalite and diorite, which are members of the Kohistan batholith, intruded into the metabasic and sedimentary rocks in the northern (upper) part of the Kohistan complex during the late Cretaceous to Miocene (Petterson & Windley,

1985; 1991).

Southern parts of the Kohistan complex consist of metabasic rocks of the Jijal and Chilas gabbroic complexes and Kamila amphibolite belt. The Chilas complex is the 300 km-long and 40 km-wide mafic-ultramafic body and it shows a thick (>10 km) stratiform body that represents a sub-arc chamber (Coward *et al.*, 1986; Khan *et al.*, 1989). More than 85% of the Chilas complex are made up of gabbronorites, which locally change to peridotites, pyroxenites, anorthosites, and two pyroxene diorites. These rocks are characterized by a calk-alkaline trend on the AFM plot and moderate FeO/MgO ratios (Khan *et al.*, 1993). Ar-Ar ages of 80 Ma were obtained from the gabbronorite in the Chilas complex (Treloar *et al.*, 1989). The Chilas complex were metamorphosed in the granulite facies conditions of 750-850 °C at 600-800 MPa in the early Cretaceous (Jan & Howie, 1980; Bard, 1983).

The Jijal complex is composed of garnet granulites and ultramafic rocks. The garnet granulites derived from gabbronorite were metamorphosed in the conditions of 697-949 °C at 1.0-1.7 GPa (Yamamoto, 1993). The high-pressure metamorphism of the Jijal complex occurred at the same time as the metamorphism of the Chilas complex. The 91.0 ± 6.3 Ma age of garnet granulites is obtained by Sm-Nd whole rock-mineral isochron (Yamamoto & Nakamura, 1996). The Jijal complex contains meta-norite relics petrogenetically similar to those of the Chilas complex at Pattan. The ultramafic rocks were carried tectonically into their present site after equilibration under high-pressure granulite facies conditions (800-850 °C, 1.2-1.4 GPa) (Jan & Howie. 1980).

The Kamila amphibolite belt (KAB) is mainly composed of amphibolites and epidote-amphibolites which were metamorphosed under 550-650 °C at 0.9-1.0 GPa before 83 ± 1 Ma, an age derived from ^{40}Ar-^{39}Ar cooling age of hornblende (Treloar *et al.*, 1990), but subordinate amounts of pyroxene granulites, intrusive sheets of tonalite-trondjhemite and hornblendites also occur. In particular, many granitic sheets intruded in the region of amphibolites have thickness of 10 km from Mandraza to 2 km north of Dasu

(Fig. 1-1 & 2-1). Jan (1988) and Treloar et al. (1990) distinguished two types of amphibolites; 1) fine to medium grained, either homogeneous or banded, and 2) medium to coarse grained and homogeneous. The former are considered as metamorphosed basic to intermediate volcanic and volcanoclastic rocks, while the latter seems to be derived from intrusive gabbros, gabbronorites and diorites. In the Indus Valley section, more than two thirds of amphibolites comprise metamorphosed basic plutonic rocks which initially intruded into amphibolites.

The KAB has been divided into two regions, such as northern and southern parts (Fig. 2-1). The northern part of the Kamila amphibolite belt (NKA) dominates amphibolites which are hydration products of the pyroxene granulites of the Chilas complex (Khan *et al.*, 1993; Treloar *et al.*, 1990), and is equivalent to "the southern Chilas complex" named by Treloar *et al.*, (1990). In this paper, the boundary between the Chilas complex and the Kamila amphibolite belt is defined by lithological change from two pyroxene granulite to amphibolites. The northern limit of occurrence of granitic sheets is defined as the boundary between the NKA and the SKA. Origin of amphibolites in the southern part of the Kamila amphibolite belt (SKA) called as Kamila shear zone (Treloar *et al.*, 1990) is controversial. Tahirkheli *et al.*, (1979), Bard *et al.*, (1980) and Bard (1983) interpreted as the metamorphosed oceanic crust intruded by subduction-related Jijal and Chilas mafic-ultramafic complexes. According to Jan (1988), both metamorphosed plutonic and volcanic basic rocks in the SKA were derived from island arc magmatism. On the other hand, the SKA could be considered to be hydrated products which were derived from the granulites of the Chilas complex judging from the presence of relict pyroxene granulites and early volcanic xenoliths in the gabbroic rocks (Yamamoto, 1993).

The other significant question of the tectonics is whether the lower crust of the Kohistan arc is the single island arc or not? Coward *et al.*, (1987) and Treloar *et al.*, (1990) proposed that the lower crust of the Kohistan arc was composed of at least two arcs. Recently, Treloar *et al.*, (1996) re-evaluated the origin of rocks of the KAB. They

suggested that the amphibolites of the KAB was not hydrated products of the gabbronorites of the Chilas complex, but was intruded by gabbronorite of the Chilas complex. However, the author believes that most of amphibolites of the KAB, at least in the Indus Valley section, are hydrated products of pyroxene granulites of the Chilas complex. Thus, field relations among rocks of the KAB, Chilas complex and Jijal complex will be described in the following chapter.

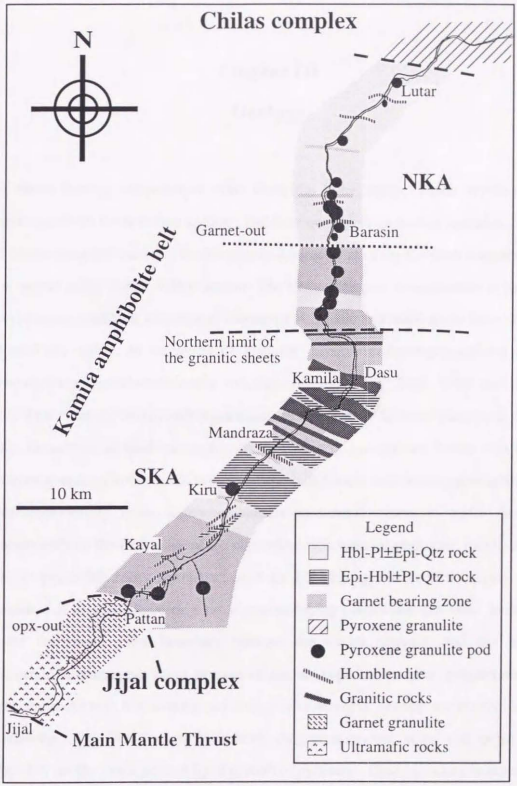

Fig. 2-1. Lithological map along the Indus Valley section. Northern limits of occurrence of orthopyroxene and garnet are shown by "opx-out" and "Garnet-out", respectively. The "opx-out" line corresponds to the complex boundary between the Jijal complex and KAB. Substantially granitic sheets with width of 8 km are distributed near Kamila. Closed circles represent the occurrence of the relict pyroxene granulite pods, and their sizes denote approximate abundance of the pods.

Chapter III

Geology

The author investigated mainly a route along the Indus valley, which provides the longest cut of the lower crustal section. The three geological units (Jijal complex, KAB and Chilas complex) that form the lower crustal component of the Kohistan complex can be observed in the Indus Valley section. The Chilas complex is composed of mainly two-pyroxene granulites with several masses of ultramafic and mafic rocks called UMA (Khan *et al.*, 1993). In the pyroxene granulite, hornblende-bearing zones are often observed along plagioclase-rich veins and pegmatitic rocks (Fig. 3-1a). In the case of the Indus Valley section, two pyroxene granulites were regionally hydrated from Lutar to the south. Occurrence of localized amphibolite formation is a ubiquitous feature within the pyroxene granulites in the Chilas complex, especially widely well developed near Shatial. Hornblende-bearing zones a few millimeters to several meters in width develop symmetrically on the both sides of the plagioclase-rich veins or pegmatitic rocks. These veins or pegmatitic rocks are characterized by NS-striking and vertical dipping. The abundance of hornblende-bearing zones accompanying plagioclase-rich veins increases toward the south. Near boundary between the Chilas complex and the KAB, hornblende-bearing zones occur in most of the outcrops. At the area, plagioclase-rich pegmatitic rocks with EW-striking and steeply dip commonly develop and clearly cut the NS-striking vein. Undeformed hornblende megacryst-bearing veins and pegmatites completely cut the fabric defined by alignment of pyroxene. Clear boundary between the Kamila amphibolite belt and the Chilas complex can not be recognized because of the gradual transition. To the south, abundance of two pyroxene granulites which occur as relict pods without hydration abruptly decrease. Intensity of hydration increases with

increasing density of the hornblende-plagioclase pegmatite. There is abundant hornblendite dyke with a few centimeters to 100-200 meter scale through the section of the Indus Valley. Variably deformed hornblendite sheets lay subparallel to tectonic foliation in the surrounding rocks. The hornblendite dykes were formed as a result of the last magmatic activity in the Chilas complex (Treloar *et al.*, 1990).

In the NKA, coarse-grained amphibolites are dominant, but abundant pyroxene granulite pods having a meter to a kilometer in diameter also occur. These rocks of the NKA are very weakly deformed, but preserve cumulate structures such as compositional banding showing grading. Igneous layering within coarse grained-amphibolites is approximately equivalent to cumulus structure of the layered gabbro in the Chilas complex and is locally preserved. From Pattan to Kiru in the southern part of the Kamila amphibolite belt, primary igneous structures are dominated by an NE-SW-striking layering and change an EW-striking northward from Kiru (Fig. 2-1). Regional trend of the mafic banding seems to continue over the boundary between the Kamila amphibolite belt and the Jijal garnet granulites. In the SKA, anastomosing shear zones so-called as the Kamila Shear Zone develop widely and degree of hydration is more intensive than the NKA (Treloar *et al.*, 1990). Pyroxene granulite pods are mostly restricted to the southern margin of the SKA, and their sizes are smaller than those of the NKA. In the SKA, pyroxene granulite pods are restricted to the southern margin of the SKA, and their sizes are much smaller than those of the NKA. Boundaries between the amphibolite and pyroxene granulite pod are not sharp in the granular coarse-grained rocks. In foliated amphibolites, coarse-grained granular pyroxene granulite pods were cut by strongly foliated amphibolites (Fig. 3-1b). Petrographical characteristics of amphibolites of the KAB are similar to that of the hornblende-bearing rocks in the pyroxene granulite of the Chilas complex. Pyroxene granulites of the Chilas complex can be correlated with pyroxene granulite pods in the KAB by means of their petrography. It suggests that amphibolites of the KAB were derived from the same rock type as pyroxene granulites of

the Chilas complex. Consequently, it is apparent that the pods of the pyroxene granulite have early stage mineralogies of the KAB mass.

Quartzo-feldspathic veins with width of several millimeters widely develop in the pyroxene granulites throughout the KAB. Occurrence of garnet, scapolite and biotite seems to be restricted in the margin of quartzo-feldspathic veins in pyroxene granulites and can be recognized as a reaction zone in the pyroxene granulite. Amphibolites, pyroxene granulites and granites contain variable grain size of garnets commonly within the KAB. These garnets in the KAB are mainly distributed in its southern margin and about 20 km wide zone from Mandraza to Barasin and included in pyroxene granulites, amphibolites and granitic rocks. To the contrary, garnet disappear in the Chilas complex along the investigated route. The garnet-bearing reaction zone does not develop along the quartzo-feldspathic vein in northern part of the NKA (Fig. 2-1). In most of case, garnet tends to occur along and/or within the feldspathic veins and its abundance and grain size decreases further from the veins.

The granitic rocks are exposed about 10 km wide in the SKA from 4 km north of Dasu to Mandraza. It contains variable types of granitoid; garnet-bearing granitic gneiss, hornblende-bearing granodiorites, epidote-bearing plagioclase-rich granitic sheets and muscovite-bearing pegmatitic tronjdhemites. The garnet-bearing granitic gneiss is widely exposed and their gneissose foliation defined by alignment of mica, especially biotite is subparallel to the foliation of the amphibolites. The plagioclase-rich granitic rocks include the amphibole-rich fine-grained amphibolites and are boudinaged commonly. Although the regional compositional layering defined by plagioclase-rich and amphibole-rich layers with centimeter to meter-scale is subparallel to the foliation of the host rocks, and in some cases, it is obliquely cut by the foliation. Because these granitic sheets commonly show boudinage structures and many buckle folds, they are considered to intrude before or during ductile deformation of amphibolites in the KAB. On the other hand, occurrence of the micaceous granitic pegmatites is completely disconcordant with the tectonic foliation

and the compositional layering of the surrounding rocks. The hornblende poikiloblast-bearing granitic pegmatites also cut these regional foliations and layerings. The geological structures show that the pegmatitic intrusion events are related to the later magmatic activity.

Pyroxene granulites are observed in the SKA adjacent to the Jijal garnet granulites near Pattan, where the boundary between pyroxene granulite and garnet granulite can be readily recognized. The garnet-bearing granulite occurs as veins, lenses, bands and patches in garnet-free pyroxene granulite (Fig. 3-1c). Although complicated boundaries between garnet-free and garnet-bearing granulites are commonly observed (see Yamamoto 1993), the primary compositional layering in pyroxene granulites is continuously preserved in garnet granulites at the boundary between garnet and pyroxene granulites. In most cases, garnetiferous veins are characterized by subhorizontal distribution at the boundary of two geological units. In the pyroxene granulite mass, the volume fraction of garnet generally increases toward the garnet granulite mass. The transitional zone between pyroxene granulites and garnet granulites has 500 m in width. The hydration of both garnet granulites and pyroxene granulites occurs along the quartzo-feldspathic vein. Based on the mineral assemblage and texture, hydrated garnet granulites can be identified as the amphibolite in the Kamila amphibolite belt. The appearance of amphibolites in the garnet granulites of the Jijal complex is quite similar to the amphibolites derived from the pyroxene granulites in the Chilas complex. The occurrence of amphibolites is similar to that of hornblende-bearing rock facies within the Chilas complex. Furthermore these appearances directly represent turn of the formation of these rocks; some part of two-pyroxene granulites changed to garnet granulites and subsequently amphibolites formed along the feldspathic veins due to hydration in both of pyroxene granulites and garnet granulites.

In summary, three geological units in the lower crust of the Kohistan arc should be identical to the only one lithology consisting of pyroxene granulites derived from

gabbronorites, although there are small amounts of amphibolite with metavolcanic origin. Pyroxene granulites were locally or regionally overprinted by garnet granulites in the deeper part of the lower crust. Pyroxene and garnet granulites alternated into amphibolites as a result of hydration in association with widely developed ductile deformation and formation of quartzo-feldspathic veins. Field relations are thought to simply represent the gradual change rather than separation as tectonic terranes.

Chapter III

Geology

The author investigated mainly a route along the Indus valley, which provides the longest cut of the lower crustal section. The three geological units (Jijal complex, KAB and Chilas complex) that form the lower crustal component of the Kohistan complex can be observed in the Indus Valley section. The Chilas complex is composed of mainly two-pyroxene granulites with several masses of ultramafic and mafic rocks called UMA (Khan *et al.*, 1993). In the pyroxene granulite, hornblende-bearing zones are often observed along plagioclase-rich veins and pegmatitic rocks (Fig. 3-1a). In the case of the Indus Valley section, two pyroxene granulites were regionally hydrated from Lutar to the south. Occurrence of localized amphibolite formation is a ubiquitous feature within the pyroxene granulites in the Chilas complex, especially widely well developed near Shatial. Hornblende-bearing zones a few millimeters to several meters in width develop symmetrically on the both sides of the plagioclase-rich veins or pegmatitic rocks. These veins or pegmatitic rocks are characterized by NS-striking and vertical dipping. The abundance of hornblende-bearing zones accompanying plagioclase-rich veins increases toward the south. Near boundary between the Chilas complex and the KAB, hornblende-bearing zones occur in most of the outcrops. At the area, plagioclase-rich pegmatitic rocks with EW-striking and steeply dip commonly develop and clearly cut the NS-striking vein. Undeformed hornblende megacryst-bearing veins and pegmatites completely cut the fabric defined by alignment of pyroxene. Clear boundary between the Kamila amphibolite belt and the Chilas complex can not be recognized because of the gradual transition. To the south, abundance of two pyroxene granulites which occur as relict pods without hydration abruptly decrease. Intensity of hydration increases with

increasing density of the hornblende-plagioclase pegmatite. There is abundant hornblendite dyke with a few centimeters to 100-200 meter scale through the section of the Indus Valley. Variably deformed hornblendite sheets lay subparallel to tectonic foliation in the surrounding rocks. The hornblendite dykes were formed as a result of the last magmatic activity in the Chilas complex (Treloar *et al.*, 1990).

In the NKA, coarse-grained amphibolites are dominant, but abundant pyroxene granulite pods having a meter to a kilometer in diameter also occur. These rocks of the NKA are very weakly deformed, but preserve cumulate structures such as compositional banding showing grading. Igneous layering within coarse grained-amphibolites is approximately equivalent to cumulus structure of the layered gabbro in the Chilas complex and is locally preserved. From Pattan to Kiru in the southern part of the Kamila amphibolite belt, primary igneous structures are dominated by an NE-SW-striking layering and change an EW-striking northward from Kiru (Fig. 2-1). Regional trend of the mafic banding seems to continue over the boundary between the Kamila amphibolite belt and the Jijal garnet granulites. In the SKA, anastomosing shear zones so-called as the Kamila Shear Zone develop widely and degree of hydration is more intensive than the NKA (Treloar *et al.*, 1990). Pyroxene granulite pods are mostly restricted to the southern margin of the SKA, and their sizes are smaller than those of the NKA. In the SKA, pyroxene granulite pods are restricted to the southern margin of the SKA, and their sizes are much smaller than those of the NKA. Boundaries between the amphibolite and pyroxene granulite pod are not sharp in the granular coarse-grained rocks. In foliated amphibolites, coarse-grained granular pyroxene granulite pods were cut by strongly foliated amphibolites (Fig. 3-1b). Petrographical characteristics of amphibolites of the KAB are similar to that of the hornblende-bearing rocks in the pyroxene granulite of the Chilas complex. Pyroxene granulites of the Chilas complex can be correlated with pyroxene granulite pods in the KAB by means of their petrography. It suggests that amphibolites of the KAB were derived from the same rock type as pyroxene granulites of

the Chilas complex. Consequently, it is apparent that the pods of the pyroxene granulite have early stage mineralogies of the KAB mass.

Quartzo-feldspathic veins with width of several millimeters widely develop in the pyroxene granulites throughout the KAB. Occurrence of garnet, scapolite and biotite seems to be restricted in the margin of quartzo-feldspathic veins in pyroxene granulites and can be recognized as a reaction zone in the pyroxene granulite. Amphibolites, pyroxene granulites and granites contain variable grain size of garnets commonly within the KAB. These garnets in the KAB are mainly distributed in its southern margin and about 20 km wide zone from Mandraza to Barasin and included in pyroxene granulites, amphibolites and granitic rocks. To the contrary, garnet disappear in the Chilas complex along the investigated route. The garnet-bearing reaction zone does not develop along the quartzo-feldspathic vein in northern part of the NKA (Fig. 2-1). In most of case, garnet tends to occur along and/or within the feldspathic veins and its abundance and grain size decreases further from the veins.

The granitic rocks are exposed about 10 km wide in the SKA from 4 km north of Dasu to Mandraza. It contains variable types of granitoid; garnet-bearing granitic gneiss, hornblende-bearing granodiorites, epidote-bearing plagioclase-rich granitic sheets and muscovite-bearing pegmatitic tronjdhemites. The garnet-bearing granitic gneiss is widely exposed and their gneissose foliation defined by alignment of mica, especially biotite is subparallel to the foliation of the amphibolites. The plagioclase-rich granitic rocks include the amphibole-rich fine-grained amphibolites and are boudinaged commonly. Although the regional compositional layering defined by plagioclase-rich and amphibole-rich layers with centimeter to meter-scale is subparallel to the foliation of the host rocks, and in some cases, it is obliquely cut by the foliation. Because these granitic sheets commonly show boudinage structures and many buckle folds, they are considered to intrude before or during ductile deformation of amphibolites in the KAB. On the other hand, occurrence of the micaceous granitic pegmatites is completely disconcordant with the tectonic foliation

and the compositional layering of the surrounding rocks. The hornblende poikiloblast-bearing granitic pegmatites also cut these regional foliations and layerings. The geological structures show that the pegmatitic intrusion events are related to the later magmatic activity.

Pyroxene granulites are observed in the SKA adjacent to the Jijal garnet granulites near Pattan, where the boundary between pyroxene granulite and garnet granulite can be readily recognized. The garnet-bearing granulite occurs as veins, lenses, bands and patches in garnet-free pyroxene granulite (Fig. 3-1c). Although complicated boundaries between garnet-free and garnet-bearing granulites are commonly observed (see Yamamoto 1993), the primary compositional layering in pyroxene granulites is continuously preserved in garnet granulites at the boundary between garnet and pyroxene granulites. In most cases, garnetiferous veins are characterized by subhorizontal distribution at the boundary of two geological units. In the pyroxene granulite mass, the volume fraction of garnet generally increases toward the garnet granulite mass. The transitional zone between pyroxene granulites and garnet granulites has 500 m in width. The hydration of both garnet granulites and pyroxene granulites occurs along the quartzo-feldspathic vein. Based on the mineral assemblage and texture, hydrated garnet granulites can be identified as the amphibolite in the Kamila amphibolite belt. The appearance of amphibolites in the garnet granulites of the Jijal complex is quite similar to the amphibolites derived from the pyroxene granulites in the Chilas complex. The occurrence of amphibolites is similar to that of hornblende-bearing rock facies within the Chilas complex. Furthermore these appearances directly represent turn of the formation of these rocks; some part of two-pyroxene granulites changed to garnet granulites and subsequently amphibolites formed along the feldspathic veins due to hydration in both of pyroxene granulites and garnet granulites.

In summary, three geological units in the lower crust of the Kohistan arc should be identical to the only one lithology consisting of pyroxene granulites derived from

gabbronorites, although there are small amounts of amphibolite with metavolcanic origin. Pyroxene granulites were locally or regionally overprinted by garnet granulites in the deeper part of the lower crust. Pyroxene and garnet granulites alternated into amphibolites as a result of hydration in association with widely developed ductile deformation and formation of quartzo-feldspathic veins. Field relations are thought to simply represent the gradual change rather than separation as tectonic terranes.

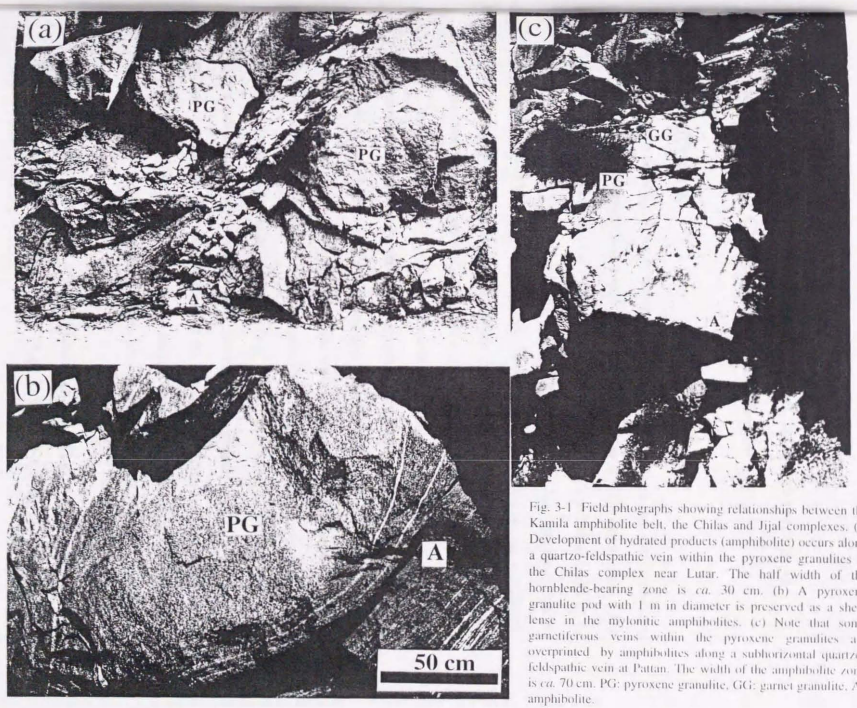

Fig. 3-1 Field phtographs showing relationships between the Kamila amphibolite belt, the Chilas and Jijal complexes. (a) Development of hydrated products (amphibolite) occurs along a quartzo-feldspathic vein within the pyroxene granulites in the Chilas complex near Lutar. The half width of the hornblende-bearing zone is *ca.* 30 cm. (b) A pyroxene granulite pod with 1 m in diameter is preserved as a shear lense in the mylonitic amphibolites. (c) Note that some garnetiferous veins within the pyroxene granulites are overprinted by amphibolites along a subhorizontal quartzo-feldspathic vein at Pattan. The width of the amphibolite zone is *ca.* 70 cm. PG: pyroxene granulite, GG: garnet granulite, A: amphibolite.

Chapter IV

Metamorphic *P-T* Paths Inferred from Al-zoning in Clinopyroxene and Plagioclase

INTRODUCTION

The Kohistan complex, lying in the north-western part of Himalaya, has been considered as a Cretaceous magmatic island arc so-called as the Kohistan arc (Tahirkheli *et al.*, 1979; Bard *et al.*, 1980; Coward *et al.*, 1982, 1986). The well-exposed lower crust rocks of the Kohistan arc has classified into three geological units: the Jijal complex, Kamila amphibolite belt and Chilas complex. Metabasic rocks of the Kohistan arc experienced complicated evolutional process including magmatism, regional metamorphism and localized ductile deformation (e.g. Coward *et al.*, 1986; Treloar *et al.*, 1990).

Yamamoto (1993) proposed a tectonic thickening model on the basis of two contrasting *P-T* paths of garnet-bearing granulites in the Chilas and Jijal complexes. The *P-T* path of the Chilas complex indicates approximately isobaric cooling at the relatively low pressure conditions, whereas that of the Jijal complex shows anti-clockwise paths at the high pressure conditions. Such anti-clockwise *P-T* paths may reflect crustal thickening due to magmatic underplating in the crust (e.g. Wells, 1980; Bohlen, 1987; Harley, 1989). It is insufficient to apply above model to the *P-T* paths obtained from only two separate complexes, because *P-T* paths for rocks of the Kamila amphibolite belt sandwiched by the Chilas and Jijal complexes has not been clarified enough. To understand the evolutional process of the lower crust of the Kohistan arc, determination of *P-T* paths of the Kamila amphibolite belt is needed.

The Kamila amphibolite belt has pyroxene granulite which have not been suffered from hydration producing amphibolites (e.g. Treloar *et al.*, 1990). The pyroxene

granulites contain pyroxene and plagioclase which preserve a distinct compositional zoning of Al. Al-zonings in clinopyroxene and plagioclase are useful for determination of *P-T* path of granulites (Anovitz, 1991), because charge-coupled two-site exchange reaction is relatively slower than one-site exchange between Mg^{2+} and Fe^{2+}. Experimentally determined diffusivities of plagioclase exchange ($NaSiCa_{-1}Al_{-1}$), jadeite exchange ($NaAlMg_{-2}$) and Ca-tschermaks exchange ($CaSiAl_{-2}$) are slow enough to retain growth zoning under high-T conditions (e.g. Yund & Snow, 1989; Sautter *et al.*, 1988). In this study, to determine the *P-T* path of the relict pyroxene granilites in the Kamila amphibolite belt, their petrographical and chemical characteristics, especially Al-zoning in clinopyroxene and plagioclase will be described. The *P-T* paths inferred from Al-zoning in clinopyroxene and plagioclase show evidence for significant crustal thickening. Then a model of crustal thickening of the Kohistan arc throughout its igneous and metamorphic evolution will be proposed.

PETROGRAPHY

The southern Kohistan complex is composed of amphibolites, pyroxene granulites and garnet granulites. These lithologies are summarized in this section. The Kohistan granulites have been briefly classified into pyroxene granulite and garnet granulite (Jan & Howie, 1980; 1981; Yamamoto, 1993). Garnet granulite occurs only in the Jijal complex and pyroxene granulite, which is important to estimate prograde *P-T* path can be found in both of the KAB and Chilas complex. Modal compositions and other petrographical characteristics are similar to each other, but various occurrences of pyroxene granulite can be observed.

Pyroxene granulite

The pyroxene granulites in the KAB are almost fine to medium grained. Locally they grade into coarser-grained rocks with a foliated texture. These textural changes are

commonly observed in same outcrop. Although foliations are rare in the pyroxene granulites in the KAB, at a strongly deformed part, alignment of pyroxene can be recognized parallel to deflected veins. Different intrusions that formed the protolith of the pyroxene granulites are extremely difficult to distinguish because no contact aureoles were formed or preserved. Replacement of pyroxene by amphibole is common and occurs at variable scales (mm-km) in the pyroxene granulites.

The pyroxene granulites in the Chilas complex are composed mainly of plagioclase (60-70 vol%), clinopyroxene (10-20 vol%), and orthopyroxene (10-20 vol%), with minor amounts of hornblende, biotite, quartz and Fe-Ti oxides. The pyroxene granulites in the KAB represent quite similar modal composition and mineral assemblage to those of the Chilas complex. Some petrographical differences of the pyroxene granulites between the KAB and Chilas complex are shown by reduced amounts of modal composition of plagioclase (50-60 vol%) (Table 4-1) and locally development of scapolite and garnet near the quartzofeldspathic veins. The pyroxene granulites show textures ranging from cumulate to granoblastic. The cumulate texture is defined by preferred alignment of euhedral and subhedral pyroxene grains with exsolution lamellae and of anorthite-rich plagioclase laths with well-developed twin (Fig. 4-1a). By contrast, granoblastic texture is defined by idioblastic, equant and polygonal pyroxene and plagioclase grains, with no shape preferred orientation (Fig. 4-1b). Gradual change from the cumulate to granoblastic texture can be commonly observed in a same thin section. Large subhedral pyroxene grains are partially or totally replaced by fine-grained polygonal pyroxene grains. Secondary small equigranular plagioclase grains develop along grain boundary between large subhedral plagioclase laths. The cumulate texture is dominant in granulites of the Chilas complex, whereas the granoblastic texture is dominant in pyroxene granulites of the KAB, where the cumulate texture is rarely preserved.

Garnet granulite

Garnet granulite is one of the typical lithology in the Kohistan arc, although the homogeneous garnet granulite does not appear in the Kamila amphibolite belt. The garnet granulites in the Jijal complex can be classified into two types; plagioclase-bearing and free types (Yamamoto, 1993). The plagioclase-bearing garnet granulites consist of garnet, clinopyroxene, plagioclase, quartz, rutile, magnetite, ilmenite, minor hornblende, epidote and scapolite. In some case, scapolite occupy similar modal composition of plagioclase. The granoblastic texture is dominant. The plagioclase-free garnet granulites consists of garnet, clinopyroxene, hornblende, rutile, magnetite, ilmenite and rare scapolite. The plagioclase-free garnet hornblendite is one of the typical lithology of the Jijal garnet granulite body and occur as a pod- or lens-shaped among the plagioclase-bearing garnet granulites. The pods and lenses of the garnet hornblendite commonly have garnet-rich rim and hornblende-rich core. The boundary between the plagioclase-bearing garnet granulites and the garnet hornblendite is marked by aligned large garnet grains (up to 3 cm in diameter) and discordant to the compositional layering present in the plagioclase-bearing garnet granulites.

Amphibolite

Jan (1988) classified the KAB into fine-grained and coarse-grained amphibolite in spite of the same mineral assemblage. Furthermore fine-grained amphibolites are classified into banded and unbanded types by Treloar *et al.*, (1990). The banded type is characterized by compositional layering consisting of hornblende-rich and plagioclase-rich layer. The compositional layering is commonly observed as a metamorphic or magmatic vein subparallel to the tectonic foliation within the shear zone. The unbanded type was interpreted as a volcanic origin (Jan. 1988, Treloar *et al.*, 1990). However, appearance of fine-grained amphibolites may be due to intensive deformation but due to original texture, because grain size reduction generally occurs in the ductile shear zone in the mylonite formation.

The dominant lithology of the KAB are undeformed or weakly deformed hornblende-plagioclase bearing coarse-grained amphibolites. Variable types of shear zones cut the amphibolites. More than two thirds of amphibolites in the Indus Valley are metamorphosed basic plutonic rocks. Most of amphibolites show the same REE pattern of the pyroxene granulite in the Chilas complex (Khan *et al.*, 1993). These signatures are resemble extensively to the undeformed pyroxene granulites of the Chilas complex in the field, because coarse pyroxene grains are partly or completely replaced by coarse amphibole grains. Because hydration reaction in the pyroxene granulites can be commonly recognized by pyroxene grains rimmed by hornblende in coarse-grained amphibolites (Yamamoto, 1993), coarse-grained amphibolite can be considered to be derived from gabbroic rocks. On the other hand, epidote-bearing fine-grained amphibolite is mainly distributed near Kamila and interlayered with granitic veins or sheets.

Amphibolites in the KAB consist of amphibole (40-60 vol%), plagioclase (30-60 vol%), epidote and quartz, with subordinate amounts of chlorite, rutile, sphene, magnetite, ilmenite and garnet. Modal compositions of rocks in the NKA and SKA are significantly different (Table 4-1). The volume fraction of plagioclase in the NKA is much greater than that in the SKA, being dependent on the appearance of idioblastic epidote only in the SKA. Garnet appears restrictedly near the plagioclase-rich vein as well as in that pyroxene granulites. Most of plagioclase in rocks having the retrogressive mineral assemblage is saussulitized (rarely sericitized) *i.e.* partly or totally replaced by fine-grained clinozoisite, albite, muscovite, and quartz. Mineral assemblages of the host pyroxene granulite due to retrograde metamorphism gradually change northward from upper amphibolite facies to greenschist facies except for the locally non-hydrated areas.

Amphibolites show two different microstructures; cumulate and granoblastic textures, which are similar to those of pyroxene granulites. The cumulate texture is characterized by large euhedral brownish to dark green hornblende with lamellae of Fe-Ti oxides, subhedral plagioclase laths with well-developed twin and interstitial quartz. In

contrast, the granoblastic texture generally develops in relatively fine-grained amphibolites within anastomosing shear zones cutting the pyroxene granulites and undeformed coarse-grained amphibolites. Mylonitic foliations and lineations in deformed amphibolites are defined by elongated fine-grained plagioclase aggregates and alignment of tabular amphibole and epidote grains (Fig. 4-1c).

MINERAL CHEMISTRY AND REACTION TEXTURES

Mineral chemistry of the pyroxene granulites and amphibolites of the Kohistan arc will be described in the following sections. The chemical compositions of the minerals were analyzed by using an electron microprobe (JEOL 733MKII) at Geological Institute, University of Tokyo. Wavelength-dispersive analyses were conducted using an accelerating voltage of 15 kV and a beam current of 12 nA. The standards used were wollastonite (Ca, Si), rutile (Ti), corundum (Al), periclase (Mg), hematite (Fe), Mn-olivine (Mn), albite (Na), adularia (K) and chromite (Cr). X-ray intensities were converted to oxide weight percentage based on the methods of Bence & Albee (1968). For pyroxene analysis, Fe^{3+} contents are estimated by stoichiometric normalization. Representative mineral analyses are shown in Tables 4-2 to 4-6.

Pyroxene granulites

Pyroxene shows different occurrences between the cumulate and granoblastic textures of pyroxene granulites. In pyroxene granulites showing the cumulate texture, coarse-grained euhedral pyroxene grains contain exsolution lamellae and blebs, which are usually parallel to their cleavage. In contrast, in rocks with the granoblastic texture, these exsolution lamellae in pyroxene are not common. Exsolution lamellae of orthopyroxene elongated parallel to (110) plane of clinopyroxene develop in the cores surrounded by exsolution-free rims (Fig. 4-2a). The brownish Fe-Ti oxide platelets and blebs in pyroxenes, especially clinopyroxene, also develop along cleavages. Magnetite inclusions occur in

cores of euhedral pyroxene grains. These observations suggest reactions at cooling stage of ferri- and titan-tschermaks components in igneous pyroxene (Bradshaw. 1989). In this paper, well-developed domains of exsolution lamellae of orthopyroxene are called as the core of the clinopyroxene grains. The rim of clinopyroxene in the NKA can be subdivided into the inner rim and the outer rim. The boundary between inner and outer rim is defined by the presence of ring-like arrays of very fine-grained quartz inclusions, whereas the quartz inclusion ring is absent in the SKA.

Clinopyroxenes is diopside, salite and augite, and orthopyroxene is hypersthene with significant amounts of Al, Ti and Fe^{3+}. Coexisting pairs of two pyroxene from pyroxene granulites with cumulate texture are illustrated in Figure 4-3. Ratio of $Mg/(Mg+Fe^{2+})$ (Mg#) of clinopyroxene and orthopyroxene ranges 0.65-0.8 and 0.5-0.7, respectively. Clinopyroxene has always higher Al-contents than coexisting orthopyroxene. The Ti-, Na- and Fe^{3+}-contents generally tend to be incorporated into clinopyroxene. There is no compositional zoning of major components (Mg, Fe and Ca) in pyroxene grains (Tables 4-2 & 4-3). On the other hand, a distinct zoning pattern of Al can be recognized in both of clinopyroxene and orthopyroxene. In the case of grains with exsolution lamellae, the Al-content in the rim of the orthopyroxene along the Indus Valley section slightly increases toward the south, whereas that in the core of orthopyroxene does not change. The Al-content of clinopyroxene grains in pyroxene granulites also increase toward the south. The atomic content of Na (cation per formulae unit) of clinopyroxenes increases from 0.028 to 0.063 from the Chilas complex to the SKA (Fig. 4-4). The Al^{3+} and Na^{+} ions of clinopyroxenes in garnet granulites of the Jijal complex are much higher than that in pyroxene granulite of the KAB and the Chilas complex.

Plagioclase in rocks with cumulate texture shows subhedral shape and develops mechanical twinning. Anorthite (An) contents of the subhedral tabular plagioclase grains range from 60 to 80 mol%. There is no regional variation of An-content in the subhedral

plagioclase grains in the single section. Distinct shape-preferred orientation and twinning plane are parallel to the alignment of pyroxene crystals, and they forms a distinct foliation. Secondary plagioclase occurs as small polygonal grains with 120° triple junctions and straight grain boundaries (Fig. 4-2c). The small polygonal plagioclase shows a more sodic composition (An_{50-60}). An-contents of large subhedral plagioclase grains does not vary at the core and slightly increase at the rim, whereas An contents of fine-grained polygonal plagioclase slightly decrease toward the rim. However, in the case of plagioclase grains which contact clinopyroxene, the zoning profile of An content generally increases toward the boundary between them.

Quartz occurs as minor phase (1-2 vol%) in pyroxene granulites. Quartz can be commonly found as a thin film between plagioclase and clinopyroxene in garnet-free pyroxene granulites from the SKA (Fig. 4-2d). In the NKA, very fine-grained quartz (1-2 μm) is included within the rim of clinopyroxene adjacent to plagioclase. This texture of quartz seems to be formed by following breakdown reactions of plagioclase (e.g. Wood 1979; Newton 1983; Anovitz 1991) as

anorthite (in plagioclase) = Ca-tschermakite (in clinopyroxene) + quartz, (1)

albite (in plagioclase) = jadeite (in clinopyroxene) + quartz. (2)

Hornblende is minor phase in pyroxene granulites. Figure 4-5 shows nomenclature of amphibole by Leake (1978). Brown to green hornblende in pyroxene granulites commonly occurs as isolated or interstitial grains. Isolated grains of hornblende are characterized by brownish colour, and higher K_2O (up to 1.5 wt%) and TiO_2 (up to 2 wt%), and lower Al_2O_3 (13-14 wt%) and Na_2O (less than 1.5 wt%) content than those of surrounding amphibolites. Higher Ti content in brown hornblende can be expected for magmatic origin coexisting with ilmenite (Otten, 1984). Occurrence of interstitial green

hornblende associated with quartz is restricted in the boundary between pyroxene and plagioclase grains (Fig. 4-2b). This occurrence suggests that hornblende and quartz are produced by hydration reaction with pyroxene and plagioclase. Interstitial hornblende is characterized by higher Al_2O_3 (15-19 wt%), being similar to tschermakitic hornblende of the surrounding amphibolites. The Al-content in hornblende continuously increases from north to south (Fig. 4-4).

Garnet in pyroxene granulites is mainly almandine-pyrope-grossular series in composition (Table 4-5). Compositional zoning can not be recognized (Fig. 4-6a). No zoning in the grain is probably caused by diffusion during high-*T* metamorphism (above 700 °C). Although X_{pyr} of garnet core in the pyroxene granulites does not vary along the Indus Valley route, X_{grs} slightly increases from 15 to 28 mol% toward the south. In the reaction zone developed along the both side of the quartzofeldspathic veins, garnet and quartz symplectite partially or totally replace the isolated pyroxene grains within the plagioclase matrix, especially orthopyroxenes (Fig. 4-2e). This texture is probably due to following garnet-forming reactions (e.g. Green & Ringwood, 1967; Newton & Perkins, 1982):

orthopyroxene + plagioclase = garnet + quartz, (3)

orthopyroxene + plagioclase = garnet + clinopyroxene + quartz, (4)

clinopyroxene + plagioclase = garnet + quartz. (5)

Amphibolites

Hornblende is significant constituent mafic mineral (46-60 vol%) in amphibolites. $Mg/(Mg+Fe^{2+})$ ratio of the hornblende with high Al_2O_3 (11-14 wt%) ranges from 0.5 to 0.7. The total Al-content (Al^{iv} + Al^{vi}) in hornblende in coarse-grained amphibolites increases toward the south (Fig. 4-4). In large hornblende grains (up to 1 mm in diameter), the total Al-content increases from the core to the rim. Fe-Ti oxide phase, especially

ilmenite, is usually rimmed by brown hornblende adjacent to plagioclase grains. Large euhedral hornblende (up to 1 mm in diameter) including Fe-Ti oxide platelets is rarely observed in rocks with the cumulate texture. Bluish-green to dark green hornblende in rocks with granoblastic texture show high Al_2O_3 contents (13-18 wt%). Chemical compositions of hornblende vary from magnesio-hornblende through tschermakitic hornblende to tschermakite in each thin section, following the nomenclature of Leake (1978). Al-content of bluish-green hornblende in the granoblastic texture continuously increases southward. Change of Al-contents in hornblende seems to be continuous between the SKA and the NKA. Consequently, it is not likely that there is a major tectonic break between the SKA and NKA masses. The low fluorine and chlorine contents of hornblende have been confirmed by many analyze of lower crustal rocks in the Kohistan arc.

Plagioclase is abundant in amphibolites of the NKA, whereas its modal composition is lower than that of hornblende in amphibolites in the SKA with increasing the volume fraction of the epidote. Coarse-grained plagioclase (500 μm - 2 mm) in rocks preserving the cumulate texture in relatively unfoliated amphibolites is characterized by a slight decrease of An-content from the core (An_{45-58}) to rim (An_{40-48}). Small amount of fine-grained (100-200 μm) plagioclase develops along the grain boundaries between large plagioclase grains (up to 1 mm), and their An-content (An_{38-43}) is lower than that of the coarse-grained plagioclase. High An-content parts in plagioclase are partially replaced by clinozoisite, albite and quartz. Plagioclase in rocks with the mylonitic texture is fine-grained and polygonal in shape (50-300 μm) with 120° triple junctions and straight grain boundaries. The An content (30 and 50 mol%) is similar to those of fine-grained plagioclase in undeformed rocks. Plagioclase with high An content (>50 mol%) is observed in the core of a porphyroclastic grain (Fig. 4-4).

Epidote is common mineral in amphibolites of the SKA. Epidote composition widely range from clinozoisite to pistasite. Idioblastic epidote grains in the SKA commonly show a normal zoning with Fe^{3+}-rich cores.

Garnet occurs only just near or in the quartzo-feldspathic veins in amphibolites. CaO content of garnet slightly increases, but MgO decreases in rocks from the north to the south (Fig. 4-4). Zoning profiles of garnet in the ductile shear zone show a discontinuous pattern between the core and the rim. Garnet in amphibolites shows idioblastic in shape and contains little inclusions. Typical X_{pyr} at the rim of garnet in amphibolites is significantly lower than that in the adjacent pyroxene granulite, though chemical compositions of garnet cores are similar in the two rock types (Fig. 4-6b). From these results, it can be inferred that the garnet core formed under granulite facies conditions before hydration, and then rims of garnet overgrew or were re-equilibrated during hydration.

ALUMINUM DISTRIBUTION IN PYROXENE

Pyroxene in pyroxene granulites of the Kohistan arc contains significant amounts of Al_2O_3, up to 2.5 wt%. It is needed to investigate the minor component and their exchange in pyroxene solid solution. The tschermak exchange ($Al_2 R^{2+}_{-1} Si_{-1}$) occurs in pyroxene, leading to the hypothetical end members Ca-, Mg- and Fe-tschermak components. Other coupled substitutions embodied by the exchange vectors are Ti-tschermak exchange ($TiAl_2 R^{2+}_{-1} Si_{-2}$), ferri-diopside exchange ($TiFe^{3+}_2 R^{2+}_{-1} Si_{-2}$), essenite exchange ($AlFe^{3+} R^{2+}_{-1} Si_{-1}$), jadeite exchange ($NaAl^{VI} R^{2+}_{-2}$) and acmite exchange ($NaFe^{3+} R^{2+}_{-2}$). The end member components considered here affecting Al-zoning in pyroxene are tschermak (Ts) $(Mg, Fe, Ca)Al_2SiO_6$, jadeite (Jd) $NaAlSi_2O_6$, acmite (Ac) $NaFe^{3+}Si_2O_6$, essenite (Es) $CaFe^{3+}AlSiO_6$, Cr-tschermak (CrTs) $CaCrAlSiO_6$, Ti-tschermak (TiTs) $CaTiAl_2O_6$,

titan-ferri tschermak $CaTiFe^{3+}{}_2O_6$ and ferric-diopside (FDi) $CaFe^{3+}{}_2SiO_6$. The Ts components for ortho- and clinopyroxene tentatively used here are treated as Mg-tschermaks (MgTs) and Ca-tschermaks (CaTs), respectively. Table 4-2 and 4-3 show the above components of ortho- and clinopyroxene, when a tetrahedral site are occupied by only Al and Si. In the assemblage of opx-cpx-pl-qtz, the Al-contents in pyroxene will be buffered by reactions (1) and (2), and tschermak substitution between ortho- and clinopyroxene as following reaction:

$$MgAl_2SiO_6 + CaMgSi_2O_6 = Mg_2Si_2O_6 + CaAl_2SiO_6. \qquad (6)$$

Figure 4-7a shows distribution of total Al-contents between ortho- and clinopyroxene. Distribution coefficient (K_D) of Al-contents of orthopyroxene to clinopyroxene is more than 1, approximately 1.3, because of significant amounts of Jd component in clinopyroxene. Mole fractions of CaTs and Jd components in clinopyroxene, which are important to clarify the *P-T* paths (Anovitz, 1991), can be evaluated to consider the effect of other ferri-titan components in pyroxene. If significant amount of Fe^{3+} exists in clinopyroxene, the amount of Jd and CaTs components should be substantially reduced by those of Ac and Es components, respectively. However, Fe^{3+} contents calculated from pyroxene stoichiometry include a large uncertainty. End-member components including Al by the ignorance of Fe^{3+} in pyroxene stoichiometry were firstly assessed. Sodium contents and (Al-Na-2Ti-Cr)/2 are equal to Jd and Ts components, respectively. Al-contents in orthopyroxene are almost equal to Ts component because of extensively small Na contents, less than detection limit of microprobe analysis. Figure 4-7b shows distribution of Ts components between ortho- and clinopyroxene. Ratio (K) of tschermak component of orthopyroxene to clinopyroxene is *c.* 1. However, at cores of the ortho- and clinopyroxene, the coefficient is obviously less than 1. Large amounts of

Fe^{3+} contents in clinopyroxene generally affect this dispersion for the K_D value. Because orthopyroxene contains the calculated very small amounts of Fe^{3+} rather than coexisting clinopyroxene (Tables 4-2 & 4-3), the amounts of Fe^{3+} also affect to the K_D value. This dispersion may reflect the presence of Ac and Es components in core of clinopyroxene. For evaluation of Fe^{3+} component effect in clinopyroxene, fractions of Al in M1 site of clinopyroxene, $\left(X_{Al}^{M1}\right)_{cpx}$, from microprobe atomic data as (Al-Cr-2Ti+Na)/2 and [Al-(2-Si)] are shown in Figure 4-8. The former is systematically higher than the latter and these differences tend to decrease from core to rim of each grain. The region above the line which represents slope = 1 in Figure 4-8 indicates the M1 site occupied by Fe^{3+} (Ac) instead of Al (Jd) or Fe^{3+} (Es) instead of Al (CaTs). Some of the difference in the NKA is therefore due to the presence of Ac and Es components in core of clinopyroxene. However, if FDi component is assessed based on normalization scheme in clinopyroxene of Anovitz (1991), above plots are mostly located on the line.

ALUMINUM ZONING IN PYROXENE AND PLAGIOCLASE

Pyroxene and plagioclase grains in the relict pyroxene granulites of the KAB preserve distinct Al-zoning profiles. The Al-zonings in orthopyroxene, clinopyroxene and plagioclase are different from the NKA to SKA in spite of the same mineral assemblages. To elucidate the equilibrium relationships between plagioclase and pyroxene during granulite facies metamorphism, results of a detailed analysis of chemical zoning of each component affecting Al-variation between plagioclase and pyroxene, especially clinopyroxene are described.

Pyroxene

In the KAB, contrasting Al-zoning patterns can be recognized between the SKA and NKA. The Al-contents in orthopyroxene of the NKA are almost constant or slightly

increase at the core and decreases at the rim toward the margin, whereas those of the SKA simply increase at the rim toward the margin (Fig. 4-9). The Al_{total} (Al^{IV}+Al^{VI}) zoning patterns in clinopyroxene are almost similar to those in orthopyroxene. Al-zoning pattern in clinopyroxene corresponds to the texture. In the NKA, the Al-content profiles at the core of large (up to 1 mm) clinopyroxene show flat patterns or small increase in Al-content from the centre to the margin of grain (Fig. 4-10). At the rim, Al-contents once increase at the inner rim and then abruptly decrease in the outer rim toward the margin of the grain. The width of Al-decreasing part at the outer rim is 20-50 μm. The Al-contents of polygonal shaped fine-grained clinopyroxene without exsolution lamellae abruptly decrease at the rim. In the SKA, Al-zoning profiles from the core of clinopyroxene is flat across the grain, being similar to that in the NKA. Reverse zoning and higher Al-contents at the rim are typical of clinopyroxene in rocks with both cumulate and granoblastic textures (Fig. 4-10). In the SKA, the Al-decreasing part at the outer rim is absent or less than 5 μm wide and difference of Al-content between a point of the maximum Al-content and outermost margin is very small in comparison with that of the NKA. Difference in Al-contents between the cores and rims of clinopyroxene in the rocks showing the cumulate texture is greater than that in the rocks with the granoblastic texture.

I need to take into consideration of change of CaTs and Jd components affecting Al zonal structure used for geothermobarometry. The contents of Fe^{3+} widely ranges from 0 to 0.06 (p.f.u). The Fe^{3+}-contents seems to be homogeneous, and locally increase just near the exsolution lamellae of iron oxides. In the SKA, Fe^{3+}-contents at the rim slightly decrease toward the outermost margin. Zoning profiles of Ti contents show flat at the core and the contents slightly decrease at the rim. Because there is no relation between Ti and Fe^{3+} contents based on the compositional zoning profiles (see Fig. 4-10), an important exchange vector as for Ti contents can be interpreted to be ($TiAl_2R^{2+}_{-1}Si_{-2}$) rather than ($TiFe^{3+}_2R^{2+}_{-1}Si_{-2}$). Sodium contents are nearly homogeneous at the core but they slightly

decrease in the outer rim in the NKA and slightly increase in the SKA toward the margin.

For each component of solid solutions, amounts of Jd and CaTs components are reduced by those of estimated Ac and Es components. Because partition coefficient of $Fe^{3+}{}_{Es}/Fe^{3+}{}_{Ac}$ is unknown, I consider zoning profiles of CaTs and Jd components by three categories as follows; (1) all Fe^{3+} is Ac component (when Fe^{3+}-contents is greater than Na-contents, a remaining Fe^{3+}-contents is treated as Es component), (2) all Fe^{3+} is Es component (when Fe^{3+}-contents is greater than Al^{iv}-2Ti-Cr, a remaining Fe^{3+}-contents is treated as Ac component) and (3) Fe^{3+} is completely FDi component. In the NKA, in the case of (1), because Na- and Fe^{3+}-contents slightly decrease in the rim, Jd component does not vary throughout the grain. Jadeite component may be reduced compared to other definitions. The zoning patterns of CaTs component should be similar trend of Al_{total} independent from the zoning patterns of Fe^{3+}. In the case of (2), amounts of CaTs component relatively decrease in comparison with the other definitions, whereas the zoning patterns are similar to those of Al-contents. Jd component is equivalent to Na-contents, because Fe^{3+} is totally consumed as Es component. In the case of (3), the shape of zoning profiles of Jd and CaTs component are equal to those of Na- and Al-contents. Consequently, Al-zoning in clinopyroxene may almost reflect the zoning pattern of CaTs component. In the SKA, in the case of (1), because zoning patterns of Na and Fe^{3+} contents show the opposite pattern, Jd component abruptly increase near the margin of the grain. Then CaTs component at the core should reduce and the difference of CaTs component between the core and outermost margin becomes smaller. In the case of (2), zoning profiles of Jd component are nearly equal to Na content due to little amounts of Ac component, and the difference of CaTs component between the core and the rim becomes greater. In the case of (3), Jd components slightly increase in the outer rim and the variation in CaTs component should be similar to that of total Al^{3+}. In any cases, both of Jd and CaTs component almost always increase toward the rim.

I briefly summarize the important end member component in clinopyroxene of pyroxene granulites in the NKA and SKA for geothermobarometrical analysis described later. The compositional trend from the core to rim in clinopyroxene (Fig. 4-8) suggests that Es and Ac components are relatively large at the core and then continuously decreases toward the rim. In the NKA, decrease in Es and Ac components toward the margin corresponds increase in FDi component, because zoning profiles of Fe^{3+}-contents are almost flat. Therefore, the ratio of Jd and CaTs components to Al cation may relatively increase in the outer rim. In the SKA, decrease in Ac and Es components from the core to rim (Fig. 4-8b) leads to increase in Jd and CaTs components from the core to the rim, because Fe^{3+}-contents decrease toward the margin of the grain. In zoning profiles of clinopyroxene in the SKA, the starting positions of the decrease in Fe^{3+}-contents toward the margin are consistent with those of increase in Na-contents rather than that of increase in Al-contents (Fig. 4-10b). It may reflects the significant effect of Ac exchange. Then the difference of Jd component between the core and the rim is much larger than that of CaTs component within the SKA. Consequently, as a component affecting the Al-zonal structure, CaTs component is the most significant in the NKA, whereas Jd component is important in the SKA.

Plagioclase

Figure 4-11 shows representative anorthite and albite zoning profiles in plagioclase adjacent to the clinopyroxene of pyroxene granulites. The variations of An content in plagioclase grains adjacent to clinopyroxene grains show different zoning patterns in comparison with that of matrix grains. In the NKA, An-content at the rim once slightly decreases and then increases toward the neighboring clinopyroxene grains. However, An-content at the rim of the plagioclase in contact with neighboring plagioclase does not significantly increase. In the SKA, An-content at the rim displays a suddenly increase.

P-T CONDITIONS

The assemblage opx-cpx-pl-qtz of pyroxene granulite pods in the KAB is typical assemblage of intermediate-*P* granulites facies metamorphism, with SiO_2-saturated basaltic compositions. The assemblage grt-opx-cpx-pl-qtz is stable in the divariant space between the lower pressure garnet-in curve and higher pressure orthopyroxene-out curve (e.g. Green & Ringwood, 1967; Hansen 1981). Although the divariant space strongly depend on whole rock chemistry, the bulk compositions of the pyroxene granulites in the studied area does not change. The garnet-in isograd in the pyroxene granulites of the Kohistan arc is located within the NKA (Fig. 2-1). This indicates that pressure condition of the northern part of the NKA were lower than those of the southern part of the NKA and SKA during granulite facies metamorphism. Yamamoto (1993) reported the complete consumption of orthopyroxene in the garnet granulite in the Jijal complex and the feature suggests that the Jijal garnet granulite underwent higher pressure metamorphism than the pyroxene granulite in the KAB.

Geothermobarometry

Anovitz (1991) proposed the geothermobarometry for granulite facies rocks using the Al-zoning in clinopyroxene and plagioclase, because Al-diffusion rate is significantly slower than R^{2+} cation diffusion. Experimentally-determined Al-diffusion coefficient in diopside suggests that Al diffusion in clinopyroxene can be negligible over geological time scales at less than 1000 °C (Sautter *et al.*, 1988). At least, late prograde to early retrograde *P-T* paths can be obtained from the Al-zoning in clinopyroxene and plagioclase (Anovitz, 1991). Fortunately, Al-contents in the clinopyroxene of the Kohistan pyroxene granulites are mostly enough high (up to 2.5 wt%) to apply the geothermobarometry. Clinopyroxene in no relation to garnet-forming reaction can used for thermobarometry, because garnet is produced by the consumption of clinopyroxene.

Metamorphic *P-T* paths were inferred from net transfer reactions (1) and (2) in pyroxene granulites in the KAB. To estimate the *P-T* path from Al-zoning in clinopyroxene and plagioclase, equilibrium relation between them must be considered. The zoning of An contents in plagioclase combined with the zoning in CaTs and Jd components in clinopyroxene provides a powerful monitor of the *P-T* path. Based on reactions (1) and (2), an increase in CaTs component in clinopyroxene should lead to decrease in An contents in plagioclase but an increase in Jd component will also lead to decrease in Ab contents. If whether Jd or CaTs components will be important in reactions (1) and (2), plagioclase grains in contact with clinopyroxene should represent a distinct zonal structure. Figure 4-12 illustrates typical relationships of compositional zoning between clinopyroxene and plagioclase. In the NKA, variations of An-content in plagioclase toward clinopyroxene is consistent with that of CaTs component, because the zoning pattern of CaTs component is always similar to that of total Al-contents. In contrast, in the SKA, assuming that an increase in Al-contents toward the margin is controlled by variations of CaTs component, the zoning pattern in An-contents is entirely inverse to the CaTs zoning pattern, and then Jd component should increase with increasing An contents toward the margin. This suggestion leads to estimate the presence of substantially Ac component at only the core in clinopyroxene in the SKA. Clinopyroxene in the SKA seems to involve significant amounts of Ac component rather than Es component based on relationship of zoning profiles between Na- and Fe^{3+}-contents (Fig. 4-10b). Then zoning profiles of Jd component should be similar to those of Al-contents. Furthermore, Al-zoning in clinopyroxene from the NKA has an inflection point where the slope of zoning changes from positive to negative (Fig. 4-12a). This inflection point is also shown in An-zoning in plagioclase of the NKA (Fig. 4-12a). On the other hand, the obvious inflection point of the Al-zoning of clinopyroxene of the SKA cannot be recognized. The inflection point is also absent in An-zoning in plagioclase of the SKA. These relations of the inflection point between clinopyroxene and plagioclase

probably suggest an equilibrium state between the growing surface of them. Consequently, the Al zonation between clinopyroxene and plagioclase can be regarded as equilibrium between them, if diffusion after growth of plagioclase and clinopyroxene is neglected.

During granulite facies metamorphism, growing surface of the clinopyroxene and plagioclase is assumed in equilibrium, because the Al-zoning in both of two minerals is consistent each other (Fig. 4-12). To calculate the metamorphic *P-T* conditions, certain point analysis from the Al-zoning of plagioclase and clinopyroxene were selected. For clinopyroxene, the following points were chosen: 1) a point A of abrupt change of Al-content between the igneous core and the metamorphic rim, 2) a point B of maximum Al-content between the inner and the outer rim, and 3) a point C of the outer margin (Fig. 4-12a). On the other hand, plagioclase does not display optical zonal structure. These points are called as 1) centre, 2) an inflection point of the An-zoning pattern, and 3) outhermost margin in each grains as points A, B, and C, respectively (see Fig. 4-12a) in plagioclase crystals. Since plagioclase grains from the SKA have no inflection point of the An-zoning profile, points of the centre and the outermost margin are called as points A and B. The equilibrium points A, B and C from the plagioclase zoning are identified as the above corresponding points of clinopyroxene grains. The selected points A, B and C can be considered to correspond to the early, peak, and later metamorphic conditions, respectively. In the SKA, the chemical compositions of the core and the outermost margin of clinopyroxene and plagioclase (points A and B in Fig. 4-12b) can be regarded to calculate the early and peak metamorphic conditions, respectively.

For determination of end member components, pyroxene is normalized to four cations and charge balanced to O = 3 by varying the ferric/ferrous ratio based on following site fractionation. All of Si is restricted to tetrahedral site. All of Ti and Cr occupy only in the M1 site. Aluminum and Fe^{3+} are equally partitioned into the tetrahedral and M1 sites. Mg and Fe are equally partitioned into the M1 and M2 sites. All of Ca and

Na are restricted to the M2 site. Although clinopyroxene in the pyroxene granulites of the Kohistan arc contains certain amounts of Es, Ac and FDi components, the estimated Fe^{3+}-contents always involve large error. To minimize uncertainties derived from the calculated Fe^{3+}-content, CaTs and Jd mole fractions in clinopyroxene used for geothermobarometer is defined as following simplified expressions:

$$X_{Jd} = X_{Na}^{M2} \cdot \left(\frac{Al}{Al + Fe^{3+}} \right)$$

$$X_{CaTs} = \frac{(Al - 2Ti - Cr - X_{Jd})}{2}$$

where X_{Jd} and X_{CaTs} are mole fractions of Jd and CaTs components, respectively. For activity model of clinopyroxene, a non-ideal mixing model of quaternary system (Di-Hd-Jd-CaTs) were followed by Anovitz (1991). Activity coefficients were obtained for a system in which the mole fractions of four components are normalized to 1. Although Fe^{3+} except for Ac component is treated as FDi components, the most of calculated values of X_{CaTs} is generally lower than X_{CaTs} defined by Anovitz (1991). In the non-ideal mixing model, activity for Jd component is nearly equal to its mole fraction (X_{Jd}) (Wood *et al.*, 1980; Gasparik, 1985; Liu *et al.*, 1995), whereas CaTs activity coefficient indicates relatively large, because the activity-composition relations for the Di-CaTs solution indicate relatively small positive deviation from ideality (Wood, 1979). Activity model for plagioclase is followed by Newton *et al.* (1980). Isopleths of $\log_{10}K$, as shown in Figure 4-13, for reactions (1) and (2) are used for determination of ranges of temperature and pressure (Anovitz 1991), and estimated *P-T* conditions are shown in Table 4-7. Figure 4-13 schematically shows *P-T* paths indicative of relative difference of pressure and temperature because of large uncertainties of the activity model and calculated mole fraction for Jd and CaTs components. Results from pyroxene granulites in the NKA

indicate that a path of increasing pressure and temperature follows decrease in pressure and temperature. The *P-T* paths in rocks of the SKA display an increase in both temperature and pressure under higher pressure conditions compared with those of the NKA.

To evaluate validity of these results, the metamorphic condition were inferred from the other geothermobarometry such as garnet-clinopyroxene geothermometer (Ellis & Green, 1979; Pattison & Newton, 1988; Ai, 1994; Gunguly *et al.*, 1996) and garnet-clinopyroxene-plagioclase-quartz geobarometer (Perkins & Newton, 1981; Moecher *et al.*, 1988; Eckert *et al*, 1993). The rim compositions were used for calculation of metamorphic condition, because garnet in the pyroxene granulite is chemically unzoned. Rim temperatures and pressures are calculated using five sets of chemical data from each sample in the garnet-quartz symplectite between clinopyroxene (or orthopyroxene) and plagioclase. Results for the SKA show higher pressure than that for the NKA (Table 4-8). This tendency is consistent with regional change of rim chemistries of pyroxenes.

Pyroxene granulites in the Kohistan arc are probably derived from the gabbronorite (Khan *et al.*, 1993). In fact, clinopyroxene with exsolution lamellae developed at the core seems to have igneous textures. Then, the magmatic temperature from the grains in the same thin section used by Al-zoning geothermobarometry was estimated to clarify *P-T* trajectories from magmatism to granulite facies metamorphism of the lower crustal rocks in the Kohistan arc. Crystallization temperature of gabbroic magma can be estimated from clinopyroxene chemistries of plus exsolution lamellae of orthopyroxene. Because clinopyroxene with exsolution lamellae is directly crystallized from basaltic magma, inferred compositions of clinopyroxene should indicate the magmatic temperature before granulite facies metamorphism. To reconstruct compositions of magmatic clinopyroxene, the centre of the core in clinopyroxene with development of the exsolution lamellae subvertical to thin section was measured by microprobe analysis using broad beam (c. 50 μm). The empirical solvus is used for thermometry (Kretz, 1982), based on temperature

dependence of Ca content in clinopyroxene coexisting orthopyroxene. The calculated temperatures of the pyroxene granulites of the Chilas complex and of the KAB are similar and to be 1113 ± 70 °C (Table 4-8).

Metamorphic temperatures of amphibolites have been estimated from the Fe-Mg partitioning geothermometer of Graham & Powell (1984) between coexisting garnet and hornblende. Metamorphic pressures of amphibolites were calculated using the garnet-hornblende-plagioclase-quartz geobarometer (Kohn & Spear, 1990). Amphibole formula were calculated using the average Fe^{3+} option of Spear & Kimball (1984) for this method. Microprobe analyses were carried out at the contacts of hornblende, plagioclase and garnet.

Table 4-9 shows results of geothermobarometries of amphibolites. Temperatures for garnet-bearing Hbl-Pl rock samples range from 570 to 730 °C in the NKA, and from 630 to 710 °C in the SKA, and no significant difference in temperature between the SKA and the NKA is obtained. However, the estimated pressure conditions of the NKA and SKA are significantly different. Deduced pressures range from 700 to 760 MPa in the NKA, and from 890 to 990 MPa in the SKA. The result obtained here is similar to the results from garnet-bearing pyroxene granulite pods already described.

Validity of calculated *P-T* paths

In general, quantitative geothermobarometry in granulites includes many uncertainties (Frost & Chacko, 1989), because it is difficult to estimate accurate peak-temperature for high grade rocks due to re-equilibration or intracrystalline diffusion in minerals crystallized under granulite facies metamorphism following amphibolites facies metamorphism. Although Al-zoning method including little effect of the intracrystalline diffusion during retrogression is a powerful tool to determine *P-T* path under high grade condition, *P-T* paths estimated by Al-zoning in clinopyroxene and plagioclase also involve some problems. The Al-zoning geothermobarometry has large uncertainties of calculated

Fe^{3+}-contents and activity model for clinopyroxene, and uncertainties propagate large error. That is, the ignorance of Es component in clinopyroxene may lead to overestimate the temperature conditions. If Ac component is large, metamorphic pressure conditions may decrease. Furthermore, relatively low concentration of Al in the rim of clinopyroxene in the NKA introduces to underestimate temperature condition due to uncertainty of Jd and CaTs activities, especially CaTs activity. In fact, results from the Al-zoning geothermobarometry show slightly lower temperature than those from the thermometry by using the garnet-bearing assemblage (Table 4-7 & 4-8). On the other hand, the pressures obtained from different thermobarometer for garnet-bearing pyroxene granulites are consistent with pressure conditions at the outermost margin of constituent minerals obtained from Al-zoning. The Al-zoning geothermobarometry provides relatively precise estimation of pressure in comparison with temperature, because two univariant lines for equilibrium (1) and (2) mainly depend on pressure. Nevertheless absolute values of calculated temperature and pressure conditions essentially contain the large error (Anovitz, 1991). However, overall *P-T* paths do not largely modified by changes in the activity model. Consequently, the estimated *P-T* paths should be qualitatively correct, for careful consideration of Al-zoning in plagioclase and clinopyroxene.

DISCUSSION

Metamorphic *P-T* trajectories of the lower crust in the Kohistan arc

I firstly summarize time relations between magmatism and metamorphism of pyroxene granulites, based on the petrographic and mineralogical characteristics. The rocks of the KAB sometimes preserve the primary igneous sedimentary structure (Treloar *et al.*, 1990). The occurrence of exsolution lamellae in cores of large grains of pyroxene indicates that pyroxene is crystallized from magma at high temperature conditions (>1000 °C) based on two-pyroxene thermometry. Beard & Lofgren (1991) considered that anhydrous pyroxene- and plagioclase-rich 'granulitic' assemblages in the Kohistan arc are igneous

residual phases derived from dehydration melting of hydrated basaltic and andestic rocks. However, the existence of pyroxenes crystallized at extremely high-*T* (>1100 °C) cannot be explained by dehydration melting of hydrous basalt. There is no evidence for dehydration reactions in rocks with the garnet-free mineral assemblage in the pyroxene granulites. The most of amphibolites in the KAB along the Indus Valley are hydration products derived from pyroxene granulites (Khan *et al.*, 1993).

Pyroxene granulites and garnet granulites were metamorphosed under granulite facies conditions after magmatic crystallization of gabbroic magma. Garnet granulites in the Jijal complex underwent higher pressure metamorphism than the pyroxene granulite (Green & Ringwood, 1967; Hansen, 1981). Therefore, the disappearance of orthopyroxene in Jijal garnet granulites is caused by high pressure conditions. The existence of a transitional zone between them (Yamamoto, 1993) indicates that the boundary is not a tectonic boundary such as a fault with a large displacement. In the transitional zone between garnet and pyroxene granulites, garnet-quartz symplectites are developed between pyroxene and plagioclase (Yamamoto, 1993). This observation suggests that the pyroxene granulite body transformed into garnet granulite under higher pressure granulite facies metamorphism. Amphibolite develops along the quartzo-feldspathic veins and locally developed shear zones which crosscut the boundary between garnet and pyroxene granulites. Consequently, the Early Cretaceous metamorphic event of the lower crust in the Kohistan arc can be divided into three major events: (1) intrusions of basaltic to intermediate arc-derived magma; (2) a subsequent formation of pyroxene and garnet granulites under the medium to the high pressure granulite facies metamorphism; and (3) amphibolitization of granulites.

Prograde paths of the NKA and the SKA rocks inferred from Al-zoning in plagioclase and clinopyroxene represent the increase in both of pressure and temperature after cooling of gabbroic magma (Fig. 4-13). The slope of *P-T* vectors of the NKA and SKA are quite similar, and maximum ΔP and ΔT are 350 MPa and 80 °C, respectively.

These prograde paths of pyroxene granulites are characterized by relatively increase in pressure rather than that in temperature. The metamorphic peak pressure in the SKA is generally higher than that in the NKA. The slope of $\Delta P/\Delta T$ of the prograde path is almost similar between the NKA and SKA. The peak metamorphic condition estimated by using grt-cpx-pl-qtz assemblage for the rocks involved the NKA and SKA are similar temperature conditions of 800 °C. These pressure conditions for rocks are slightly lower than the peak conditions deduced from Al-zoning patterns.

In Figure 4-14, I can recognize retrograde paths deduced from Al-zoning in clinopyroxene of the NKA. For high-grade rocks, because diffusion rates in garnets may be fast enough to obliterate pre-existing compositional zoning (e.g. Lasaga, 1983; Elphick *et al.*, 1985; Chakraborty & Ganguly, 1990) and isothermal segments of the *P-T* path will be retained. Therefore, *P-T* estimates obtained using grt-cpx-pl-qtz assemblage for the pyroxene granulite within the NKA represent retrograde conditions of granulite facies metamorphism. *P-T* trajectories from the NKA suggest that rocks of the NKA underwent retrograde metamorphism at high temperature after the peak granulite facies metamorphism. In fact, pressure conditions determined from the compositions at the rim of minerals by above two methods are quite similar. The early retrograde path in the NKA can be inferred to involve a decrease in pressure at nearly same constant temperature, namely the isothermal decompression path. This path suggests that pyroxene granulites of the NKA underwent rapid exhumation during granulite facies metamorphism and the uplift rate was relatively rapid compared with Precambrian granulite terranes such as Enderby Land, Antarctica (Ellis, 1987).

Peak *P-T* conditions in the SKA deduced from two methods are combined with that of amphibolites to define the retrograde path in the SKA. The amphibolites formed through isobaric cooling of the pyroxene granulites into the amphibolite facies metamorphic conditions (610-740°C at 900-990 MPa) following the peak granulite facies metamorphism. Such an isobaric cooling (IBC) path is commonly reported on many

granulite terranes (*e.g.* Bohlen, 1987; Harley, 1989). This isobaric cooling path is supported by the occurrence of kyanite in the SKA (Bard, 1983; Yamamoto, 1993). Estimated temperature conditions (550-730 °C) of amphibolites in the NKA are slightly lower than retrograde temperature (770-830 °C) to the pyroxene granulite, whereas pressure conditions of them are quite similar (*ca.* 730 MPa). The *P-T* trajectory of the rocks of the NKA following the retrograde granulite metamorphism is isobaric cooling, being similar to the retrograde path of the SKA during hydration of granulites. In conclusion, the whole *P-T* paths of the NKA and SKA are clockwise and anti-clockwise ones, respectively.

Crustal thickening model for the lower crust in the Kohistan arc

Prograde paths of different structural level were documented and suggest that the significant loading occurred in a regional granulite terrane in the Kohistan arc. Prograde *P-T* paths of the NKA and SKA should provide a constraint on the evolutional processes of the lower crust of the Kohistan complex. Prograde *P-T* paths both of the NKA and SKA show a large pressure increase which indicates crustal thickening, consistent with previous papers of the southern area of the Kohistan complex (Yamamoto, 1993; Jan & Karim, 1995). In this study, at least ~300 MPa increase in the load pressure was estimated. The crustal thickening is equivalent to loading of materials of about 10 km thickness over rocks already buried at depths of 15-20 km.

In general, causes of such crustal thickening have been regarded as to be either continent-continent collision (England & Thompson, 1984) or magmatic accretion beneath or within pre-existing crust (Wells, 1980; Bohlen, 1987; Harley, 1989). The crustal thickening event has been documented in a few granulite terranes formed in subduction-related magmatic arc. The Fiordland complex of New Zealand is most suitable example compared with the Kohistan complex because of many similar characteristics such as Cretaceous magmatic arc, granulite derived from gabbro, clinopyroxene showing Al zonal

structure, high-*P* metamorphic overprint and late amphibolitization (cf. Bradshaw, 1989; Oliver, 1990). Metamorphic pressure at the base of the section is consistency in 1.2-1.5 GPa for Kohistan and Fiordland. Bradshaw (1989) interpreted that the crustal thickening of the Fiordland complex was caused by overthrusting due to onloading of ~20 km thick slab. On the other hand, Brown (1996) proposed a different model of which magmatic loading resulted in the crustal thickening. According to his suggestion, as magmatic sheets horizontally emplaced in the crust, country rocks beneath the magma chamber subside passively in response to the weight of the magma and records higher pressure metamorphism.

A crustal thickening model is proposed for the lower crust of the Kohistan island arc in the Early Cretaceous due to magmatic accretion within the middle crust, from following geological considerations.

(1) Most of the exposed lower crust in the Kohistan arc, at least along the Indus Valley, is composed of metaplutonic rocks with gabbroic origin. There is no evidence for a large supracrustal rocks tectonically brought to the deeper zone of the crust. Magmatically thickened crust should be almost composed of metaigneous rocks of identical to mafic composition (Bohlen, 1987, 1991). Evidence of the thrusting under granulite facies condition cannot be recognized between the KAB and neighboring geological units, and the boundaries seem to be continuous.

(2) Prograde metamorphic *P-T* paths of the relict pyroxene granulites throughout the KAB represent increasing pressure with increasing temperature. Increasing pressure paths may reveal the magma loading above the pre-existing gabbroic crust. The Matum Das tonalite of the Kohistan batholith, which represents higher structural level of the Kohistan arc (Fig. 1-1), dated 102 Ma on the basis of Rb-Sr whole rock isochrons (Petterson & Windley, 1985) is possible source of the magma loading during the granulite facies metamorphism. Garnet granulites in the Jijal complex has been transformed from pyroxene granulites during increasing pressure, because the compositional layering in

pyroxene granulites is continuous across the boundary between garnet and pyroxene granulites. In contrast, in the case of thickened crust due to magmatic underplating at the base of the crust, the metamorphic *P-T* path should be expected to show nearly isobaric cooling caused by thermal relaxation from the perturbed geothermal gradient, unless high density materials directly bring on the base of crust.

(3) The prograde paths described in this study reveal that gabbroic masses once set at the depth. Some igneous clinopyroxene began to overgrow under granulite facies conditions near 600 MPa (~20 km in depth), which corresponds to the middle crustal depth. It indicates that large amount of gabbroic magma intruded into the pre-existing gabbroic crust at middle crustal depth. Although the Kohistan batholith is another possible loading source, most of plutons in the Kohistan batholith have younger age corresponding to the Andean type stage (Petterson & Windley, 1985).

(4) Based on the whole rock chemistry and geochronological data, Khan *et al.* (1993) suggested that the gabbronorite of the Chilas complex may be even younger than basic plutons in the Kamila amphibolite belt. The oldest age of the lower crust rocks in the Kohistan arc is from the Jijal complex based on an L-shaped Ar-Ar spectra with a plateau at 120 Ma (Treloar *et al.*, 1989), whereas U-Pb zircon age of the gabbronorite in the Chilas complex which is structurally high level is 84 Ma (Zeitler *et al.*, 1981). Then metabasic rocks in the KAB cooled through 500 °C by 76 ± 4 Ma on the basis of Ar-Ar spectra of hornblende grains (Wartho *et al.*, 1996). Relatively older gabbronorites are forced to shift downward accommodated by magmatic loading under granulite facies metamorphism. If the Sm-Nd whole rock-mineral isochron 91.0 ± 6.3 Ma age of Jijal garnet granulites (Yamamoto & Nakamura, 1996) represents the formation age of garnet granulites, an origin of garnet granulites in the Jijal complex could be caused by overprint of high-*P* metamorphism due to the magma loading.

These suggestions clearly indicate that crustal thickening process is caused by gabbroic accretion at middle crustal depth in the Kohistan arc. As another example of

crustal thickening in the subduction-related magmatic arc, Barrovian metamorphism in the Coast Plutonic complex, North American Cordillera is also considered to be the products of magma loading (Brown & Walker, 1993). However, the Kohistan arc has some different features against these terranes; moderately to subvertical dipping magmatic foliation, largely exposed garnet granulites and absence of the highest grade unit within the core of the complex. Most of these differences are probably derived from different exhumation mechanism. Magmatically thickened crusts of the Fiordland complex and the Coast Plutonic complex were exhumed by rapid extensional unroofing or isostasy to expose the highest grade part (Gibson *et al.*, 1988; Brown, 1996; Brown & Walker, 1993), whereas the lower crust of the Kohistan arc was tectonically eroded during the collision between the Kohistan arc and the Asian plate at the back arc (Coward *et al.*, 1986; Pudsey *et al.*, 1985). Therefore, early crustal thickening process before exhumation may be common feature of subduction-related magmatic arc at the continental margin. Magma loading model is one of the most important processes in the subduction-related magmatic arcs.

Implication of contrasting retrograde P-T paths

Overall *P-T* trajectories revealed that the same prograde paths and following different retrograde paths are obtained in a regional granulite terranes. One is no retrograde path from the SKA and another is clockwise (CW)-ITD path from the NKA under granulite facies condition. Bohlen (1991) concluded that ACW-IBC paths for granulites were caused by 1) episodic igneous intrusion within all levels of the crust, 2) thickening of the crust by magmatic underplating, 3) slow exhumation as a result of the formation of the high density garnet-rich deep crust, and 4) exhumation due to a later tectonic event in no relation to the formation of the granulite. In the Kohistan arc, the existence of garnet granulite in the deeper zone and of lower crustal rocks with magmatic origins are in good agreement with his suggestions. The CW-ITD path in the presence of mantle-derived

additions should reflect a process of tectonic thinning such as crustal extension following the crustal thickening. For example, granulites from Scourie complex, Scotland (Sills & Rollinson, 1987) and Serre, Calabria, northern Italy (Schenk, 1984) show that ITD at high temperature in the range 800-850 °C is followed by IBC. In such cases, the overall *P-T* paths of each granulite terrane are similar for all depths represented in the terrane. However, rocks of two regions located in the continuous lower crustal sequence in the Kohistan arc before or during amphibolitization record the different retrograde *P-T* paths. Hence, the model of the crustal thinning following the crustal thickening is not appropriate for retrograde path of the NKA.

Harley (1989) proposed that different *P-T* paths are generated in the same tectonic setting are possible depending upon the location of the pre-existing rock mass relative to the zone of magmatic accretion. According to his model, rocks in the SKA would be situated beneath main magmatic accretion zone during granulite facies metamorphism. Then the *P-T* path of rocks situated above the accretion zone should be different from the ACW path and probably experience the ITD path. In rocks above the magmatic accretion, decompression might be expected after the peak temperature due to isostatic response of the slightly thickened crust. In summary, the origin of separating paths is possible to be considered in the same tectonic setting where felsic magma intruded within the pre-existing gabbroic crust. Indeed, there are major granitic sheets in width of 10 km between the NKA and the SKA. The granitic sheets can explain the origin of contrasting retrograde *P-T* paths from the single crustal section of the Kohistan arc. Because deformation features of garnet-bearing and hornblende-bearing granitic rocks is similar to those of surrounded amphibolites, the formation of shear zones postdates the main granitic intrusion. The forming age of granitic rocks might be expected before the cooling of deformed rocks because the $^{40}Ar/^{39}Ar$ dating of hornblende in the deformed amphibolite is 83 ± 1 Ma (Treloar *et al.*, 1980). If the felsic magmas intrude within the gabbroic crust, isostatic equilibrium of the mass above the granitic rocks should be

emphasized because the granitic intrusion is relatively lighter materials in comparison with that of gabbroic component. However, formation age of granitic rocks is unclear and the field occurrence of some parts of the granitic sheets such as micaceous granitic and hornblende-bearing pegmatitic rocks often cut the deformation textures developed in amphibolites. More investigation, in especially accurate dating of these granitic rocks, is needed to check the evaluation of the tectonic model.

Table 4-1. Representative modal compositions of pyroxene granulites and amphibolites in the Kamila amphibolite belt

Sample No.	Pl	Epi	Opx	Cpx	Hbl	Qtz	Bt	Grt	Opq
NKA									
Pyroxene granulite									
SM7	60.1	-	9.9	23.8	1.9	0.4	-	-	3.9
LT8	59.4	-	18.0	20.1	1.3	0.7	-	-	0.5
1408	58.4	-	8.0	10.0	19.0	2.1	-	0.2	2.3
Amphibolite									
CH1	59.5	-	-	-	37.6	0.8	-	-	2.0
1406	47.0	-	7.6	6.1	34.2	2.3	1.4	0.5	0.7
CH2	46.2	-	-	-	44.6	2.8	0.6	-	5.8
CH2"	46.2	-	-	-	42.4	2.5	0.2	6.7	2.0
SKA									
Pyroxene granulite									
PL4	54.1	-	10.1	22.4	8.2	2.5	0.1	-	2.6
PA9	54.6	-	21.0	21.1	0.4	2.0	-	-	1.0
Amphibolite									
KY2-1	33.1	1.1	-	-	63.6	1.3	0.3	-	0.6
KY15	37.7	1.8	-	-	45.0	14.8	-	-	0.8
PU4	36.1	5.1	-	-	52.5	4.4	-	0.5	1.6
PA3	28.7	9.0	-	-	56.4	2.8	1.2	1.2	0.7

Values in volume %.

Abbreviations: Pl, plagioclase; Epi, epidote; Opx, orthopyroxene; Cpx, clinopyroxene; Hbl, hornblende; Qtz, quartz; Bt biotite; Grt, Garnet; Opq, opaque minerals.

Modes of samples were measured by counting 3000 points covering the whole of one section from each samples.

Table 4-2. Representative chemical compositions of orthopyroxene in pyroxene granulite

	Chilas complex		NKA								SKA			
Sample No.	SM7		LT3		LT8		1408		PL4		P8		PU5	
	core	rim	core	rim	core	rim	core	rim	core	rim	core	rim	core	rim
SiO_2	53.03	53.36	50.81	51.21	53.15	53.65	49.69	50.32	51.01	51.42	50.03	49.77	51.00	49.72
Al_2O_3	2.70	2.25	2.38	1.47	2.49	2.05	2.79	2.53	2.12	2.60	2.56	3.10	2.99	4.36
TiO_2	0.09	0.08	0.11	0.10	0.14	0.04	0.04	0.05	0.00	0.03	0.10	0.06	0.08	0.05
FeO*	20.90	19.68	24.63	24.55	19.97	19.48	28.60	27.37	25.63	25.02	28.46	28.78	26.59	26.34
MnO	0.56	0.51	0.83	0.88	0.45	0.46	0.86	0.80	0.57	0.58	0.73	0.67	0.65	0.74
MgO	23.15	23.43	20.65	20.42	23.76	24.09	17.59	17.60	19.78	19.83	17.45	17.08	18.41	17.50
CaO	0.56	0.46	0.52	0.62	0.71	0.54	0.53	0.59	0.47	0.49	0.54	0.37	0.71	0.93
Na_2O	0.01	0.00	0.01	0.01	0.02	0.02	0.00	0.01	0.02	0.00	0.03	0.01	0.04	0.04
Cr_2O_3	0.00	0.01	0.00	0.00	0.04	0.02	0.00	0.03	0.02	0.04	0.00	0.00	0.01	0.00
Total	101.00	99.77	99.94	99.25	100.73	100.37	100.10	99.30	99.63	100.00	99.90	99.84	100.47	99.68
O=6[†]														
Si	1.940	1.969	1.911	1.943	1.941	1.963	1.903	1.939	1.934	1.940	1.921	1.914	1.931	1.899
Al	0.116	0.098	0.106	0.066	0.107	0.089	0.126	0.115	0.095	0.115	0.116	0.141	0.133	0.196
Ti	0.003	0.002	0.003	0.003	0.004	0.001	0.001	0.001	0.000	0.001	0.003	0.002	0.002	0.001
Fe^{3+}[††]	0.000	-	0.067	0.042	0.003	-	0.065	0.005	0.037	0.002	0.040	0.028	0.003	0.005
Fe^{2+}[††]	0.639	0.607	0.708	0.737	0.607	0.596	0.850	0.877	0.776	0.787	0.874	0.898	0.839	0.837
Mn	0.017	0.016	0.026	0.028	0.014	0.014	0.028	0.026	0.018	0.018	0.024	0.022	0.021	0.024
Mg	1.262	1.289	1.158	1.155	1.294	1.314	1.004	1.011	1.118	1.115	0.999	0.980	1.039	0.997
Ca	0.022	0.018	0.021	0.025	0.028	0.021	0.022	0.025	0.019	0.020	0.022	0.015	0.029	0.038
Na	0.001	0.000	0.000	0.000	0.001	0.002	0.000	0.001	0.001	0.000	0.002	0.001	0.003	0.003
Cr	0.000	0.000	0.000	0.000	0.001	0.001	0.000	0.001	0.000	0.001	0.000	0.000	0.000	0.000
Total	4.000	4.000	4.000	4.000	4.000	4.000	4.000	4.000	4.000	4.000	4.000	4.000	4.000	4.000
X_{MgTs}	0.055	0.047	0.016	0.009	0.048	0.043	0.029	0.053	0.029	0.055	0.035	0.055	0.063	0.095
X_{MgTiTs}	0.005	0.004	0.006	0.006	0.008	0.002	0.002	0.003	0.000	0.002	0.006	0.003	0.005	0.003
Mg#[‡]	0.664	0.680	0.621	0.611	0.681	0.688	0.541	0.536	0.590	0.586	0.533	0.522	0.553	0.544

*: FeO was calculated as total iron

†: Cation was calculated based on 6-oxygens

††: Fe^{2+} and Fe^{3+} were calculated based on pyroxene stoichiometry

‡: Mg#=Mg/(Mg+Fe^{2+}) in atomic

Table 4-3. Representative chemical compositions of clinopyroxene in pyroxene granulite

	Chilas complex			NKA							SKA								
Sample No.	SM7			LT8			D8			PL4	P5			P6			PU5		
	A	B	C	A	B	C	A	B	C	core[4]	A	B	A	A	B	A	A	B	A	B
SiO_2	50.53	49.90	51.10	51.21	51.44	52.25	51.64	50.88	52.10	50.08	51.42	50.40	50.34	50.15	50.71	50.09	51.12	51.12	
Al_2O_3	3.49	3.87	2.56	3.55	4.37	2.61	3.18	3.88	2.95	3.29	3.01	4.27	3.87	4.43	3.23	4.42	4.18	4.61	
TiO_2	0.36	0.38	0.24	0.49	0.54	0.30	0.22	0.25	0.14	2.06	0.21	0.30	0.32	0.40	0.27	0.40	0.36	0.42	
FeO[1]	9.74	10.48	9.37	8.26	8.45	7.33	10.34	11.76	11.78	17.76	10.24	10.65	10.34	9.22	11.20	11.40	11.19	9.58	
MnO	0.36	0.44	0.38	0.12	0.26	0.08	0.33	0.29	0.32	0.36	0.25	0.29	0.20	0.15	0.27	0.36	0.39	0.31	
MgO	12.48	12.29	13.01	13.65	13.20	13.68	12.09	11.00	11.66	13.21	12.42	11.42	11.70	11.94	11.36	10.66	11.13	11.46	
CaO	21.66	20.88	21.75	22.84	21.84	22.86	21.76	21.18	21.33	13.91	21.59	20.94	21.76	21.80	22.02	21.27	21.45	21.30	
Na_2O	0.51	0.50	0.43	0.52	0.57	0.50	0.61	0.57	0.64	0.43	0.59	0.62	0.65	0.63	0.53	0.59	0.78	0.87	
Cr_2O_3	0.02	0.00	0.00	0.01	0.00	0.08	0.03	0.04	0.03	0.01	0.05	0.00	0.03	0.06	0.03	0.00	0.04	0.07	
Total	99.15	98.74	98.84	100.64	100.67	99.68	100.21	99.85	100.95	101.08	99.78	98.89	99.20	98.79	99.62	99.20	100.64	99.74	
Oxh[2]																			
Si	1.904	1.891	1.929	1.886	1.897	1.941	1.930	1.921	1.942	1.888	1.927	1.911	1.900	1.893	1.915	1.903	1.909	1.916	
Al	0.155	0.173	0.114	0.154	0.190	0.114	0.140	0.173	0.130	0.146	0.133	0.191	0.172	0.197	0.144	0.198	0.184	0.203	
Ti	0.010	0.011	0.007	0.013	0.015	0.008	0.006	0.007	0.004	0.058	0.006	0.008	0.009	0.011	0.008	0.011	0.010	0.012	
Fe^{2+}	0.055	0.060	0.047	0.083	0.027	0.023	0.031	0.012	0.024	0.000	0.043	0.015	0.057	0.037	0.050	0.016	0.034	0.004	
Fe^{3+}	0.252	0.272	0.248	0.171	0.233	0.205	0.292	0.359	0.343	0.560	0.278	0.322	0.269	0.254	0.304	0.346	0.316	0.296	
Mn	0.011	0.014	0.012	0.004	0.008	0.002	0.010	0.009	0.010	0.011	0.008	0.009	0.006	0.005	0.009	0.012	0.012	0.010	
Mg	0.701	0.694	0.732	0.749	0.726	0.758	0.674	0.619	0.648	0.743	0.694	0.646	0.658	0.672	0.640	0.604	0.619	0.639	
Ca	0.874	0.848	0.880	0.901	0.863	0.910	0.871	0.857	0.852	0.562	0.867	0.851	0.880	0.882	0.891	0.866	0.858	0.853	
Na	0.038	0.037	0.032	0.037	0.041	0.036	0.044	0.042	0.047	0.031	0.043	0.046	0.047	0.046	0.039	0.044	0.057	0.063	
Cr	0.000	0.000	0.000	0.000	0.000	0.002	0.001	0.001	0.001	0.000	0.001	0.000	0.001	0.002	0.002	0.000	0.001	0.002	
Total	4.000	4.000	4.000	4.000	4.000	4.000	4.000	4.000	4.000	4.000	4.000	4.000	4.000	4.000	4.000	4.000	4.000	4.000	
X_{Ca}	0.031	0.037	0.020	0.017	0.051	0.024	0.034	0.055	0.032	0.000	0.027	0.060	0.036	0.052	0.029	0.061	0.045	0.055	
X_{Na}	0.028	0.027	0.022	0.024	0.036	0.030	0.036	0.039	0.039	0.031	0.033	0.042	0.036	0.039	0.029	0.040	0.048	0.062	
$X_{Ca(M2)}$	0.021	0.021	0.013	0.027	0.030	0.016	0.013	0.014	0.008	0.117	0.012	0.017	0.018	0.023	0.015	0.023	0.020	0.025	
X_{Fe}	0.045	0.051	0.038	0.070	0.022	0.017	0.023	0.009	0.017	0.000	0.032	0.012	0.045	0.030	0.040	0.013	0.025	0.003	
X_{Mn}	0.010	0.009	0.009	0.013	0.005	0.006	0.008	0.003	0.007	0.000	0.010	0.003	0.012	0.007	0.010	0.003	0.009	0.001	
Mg#	0.735	0.719	0.747	0.814	0.757	0.787	0.697	0.633	0.654	0.570	0.714	0.667	0.709	0.726	0.678	0.636	0.662	0.683	

A = core, B = boundary between inner and outer rims, C = outermost margin[3] ; FeO* was calculated as total iron

[1]: FeO was calculated as total iron

[2]: Cation was calculated based on 6-oxygens

[3]: Fe^{3+} and Fe^{2+} were calculated based on pyroxene stoichiometry

[4]: Mg#=Mg/(Mg+Fe^{2+}) in atomic

[5]: Igneous core without exsolution lamellae

Table 4-4. Representive chemical compositions of plagioclase in pyroxene granulites

	Chilas complex			NKA						SKA					
Sample No.	SM7			LT3			D8			PL4		P8		PU5	
	A	B	C	A	B	C	A	B	C	A	B	A	B	A	B
SiO_2	51.38	54.57	50.75	54.87	55.63	53.71	56.70	56.77	48.70	53.79	57.51	54.08	53.87	55.16	53.75
Al_2O_3	31.64	29.28	31.54	29.59	29.11	30.29	27.56	27.96	32.74	30.14	30.88	28.62	28.79	28.24	29.16
CaO	14.22	11.64	14.53	11.56	11.31	13.10	10.04	10.07	15.59	12.48	13.49	11.35	11.63	10.75	11.89
Na_2O	3.15	3.74	2.82	4.47	4.61	3.62	5.20	5.60	2.07	4.19	3.71	5.12	4.92	5.14	4.75
K_2O	0.19	0.31	0.12	0.25	0.31	0.22	0.44	0.42	0.09	0.15	0.18	0.23	0.16	0.29	0.18
Total	100.58	99.53	99.26	100.73	100.96	100.43	99.94	100.78	99.19	100.25	100.76	99.40	99.32	99.57	99.73
O=8[1]															
Si	2.316	2.460	2.297	2.451	2.476	2.392	2.543	2.523	2.231	2.400	2.362	2.455	2.448	2.493	2.435
Al	1.681	1.556	1.700	1.558	1.527	1.605	1.457	1.466	1.768	1.600	1.637	1.531	1.543	1.504	1.557
Ca	0.687	0.562	0.712	0.553	0.540	0.631	0.483	0.480	0.765	0.602	0.650	0.552	0.567	0.520	0.577
Na	0.276	0.327	0.250	0.387	0.398	0.315	0.453	0.483	0.184	0.365	0.324	0.450	0.433	0.451	0.417
K	0.011	0.018	0.007	0.014	0.018	0.012	0.025	0.024	0.005	0.009	0.010	0.013	0.009	0.016	0.011
	4.970	4.923	4.965	4.963	4.958	4.956	4.961	4.976	4.954	4.976	4.983	5.001	5.001	4.984	4.997
An	0.706	0.620	0.735	0.580	0.565	0.658	0.503	0.487	0.802	0.617	0.661	0.544	0.562	0.527	0.574
Ab	0.283	0.361	0.258	0.405	0.417	0.329	0.471	0.489	0.193	0.374	0.329	0.443	0.429	0.457	0.415
Or	0.011	0.020	0.007	0.015	0.018	0.013	0.026	0.024	0.006	0.009	0.010	0.013	0.009	0.016	0.011

[1] Cations were calculated based on 8-oxygens

A, B and C are defined in text

Abbreviations: An = anorthite; Ab = albite; Or = orthoclase

Table 4-5. Representative chemical compositions of garnet in pyroxene granulites

Sample No.	NKA								SKA			
	1205		U3		D8		1408		PL2		P5	
	core	rim	core	rim	core	rim	core	rim	core	rim	core	rim
SiO_2	39.24	38.44	38.85	39.08	39.22	38.84	38.17	38.23	38.67	38.58	39.34	39.18
Al_2O_3	21.34	21.36	20.84	21.20	22.22	22.03	21.37	21.36	20.84	21.41	21.51	21.77
TiO_2	0.02	0.02	0.01	0.12	0.06	0.02	0.08	0.10	0.07	0.10	0.06	0.08
FeO*	24.44	24.55	23.48	23.30	23.65	25.01	24.92	24.58	24.43	24.17	22.94	24.58
MnO	1.11	0.99	1.65	1.58	0.83	1.06	0.80	0.84	0.72	0.48	0.55	0.64
MgO	8.30	7.95	7.13	7.18	7.15	7.27	7.05	7.03	7.29	7.15	8.12	8.02
CaO	5.71	6.61	7.81	7.10	7.11	7.10	6.98	6.93	7.71	7.70	8.02	6.73
Na_2O	0.00	0.01	0.00	0.01	0.02	0.01	0.02	0.01	0.01	0.00	0.02	0.00
Total	100.16	99.92	99.77	99.56	100.26	101.34	99.39	99.08	99.73	99.58	100.55	101.00
O=12**												
Si	3.016	2.974	3.012	3.024	2.981	2.965	2.978	2.988	2.988	2.982	3.003	2.988
Al	1.933	1.948	1.905	1.934	1.998	2.003	1.965	1.967	1.898	1.950	1.935	1.958
Ti	0.001	0.001	0.005	0.007	0.004	0.004	0.005	0.006	0.004	0.006	0.003	0.005
Fe***	1.571	1.588	1.522	1.508	1.569	1.585	1.626	1.606	1.579	1.562	1.464	1.568
Mn	0.072	0.065	0.108	0.104	0.052	0.064	0.053	0.055	0.047	0.031	0.035	0.042
Mg	0.951	0.917	0.824	0.828	0.853	0.828	0.820	0.818	0.840	0.834	0.924	0.912
Ca	0.470	0.547	0.648	0.589	0.558	0.572	0.584	0.580	0.638	0.638	0.656	0.550
Na	0.001	0.003	0.000	0.002	0.001	0.000	0.003	0.005	0.001	0.001	0.003	0.000
Alm	0.513	0.509	0.490	0.498	0.518	0.520	0.527	0.525	0.499	0.490	0.476	0.510
Py	0.310	0.294	0.266	0.273	0.281	0.272	0.266	0.267	0.281	0.281	0.300	0.297
Gr	0.153	0.176	0.209	0.194	0.184	0.188	0.189	0.190	0.213	0.214	0.213	0.179
Sp	0.024	0.021	0.035	0.034	0.017	0.021	0.017	0.018	0.016	0.011	0.011	0.014
Mg#****	0.377	0.366	0.351	0.354	0.356	0.343	0.335	0.338	0.282	0.295	0.387	0.368

*: FeO was calculated as total iron

**: Cation was calculated based on 12-oxygen

***: Fe is assumed to be Fe^{2+}

****: Mg#=Mg/(Mg+Fe) in atomic

Abbreviations: Alm, almandine; Py, pyrope; Gr, grossular; Sp, spessartine.

Table 4-6. Representative chemical compositions of hornblende in amphibolites

Sample No.	SKA						SKA									
	CH1		CH2		CH4		DU2		MA2		KY25		KY15		PA3	
	rim	core	rim	core	rim	core	rim	core	rim	core	rim	core	rim	core	rim	core
SiO_2	42.74	42.05	42.12	42.17	42.29	42.90	41.77	42.15	41.61	41.89	41.75	42.53	40.80	40.72	44.27	42.77
Al_2O_3	16.23	15.89	14.96	14.37	13.97	13.90	15.35	13.99	16.83	16.75	16.89	15.98	17.04	16.39	17.18	16.59
TiO_2	0.83	0.57	0.96	1.07	0.90	1.02	0.73	0.78	0.61	0.55	0.33	0.84	0.34	0.66	0.42	0.77
FeO*	15.10	16.87	16.33	15.95	17.01	17.41	14.83	14.22	17.35	17.77	17.17	14.09	15.55	16.42	12.83	12.98
MnO	0.10	0.26	0.29	0.28	0.22	0.20	0.26	0.28	0.00	0.07	0.27	0.29	0.18	0.22	0.21	0.23
MgO	9.28	8.87	9.07	9.11	8.79	9.49	9.92	10.91	7.98	8.17	8.00	9.53	8.71	8.69	9.78	10.23
CaO	11.23	10.76	11.30	11.44	10.96	10.78	10.65	10.57	10.21	10.56	10.87	10.89	10.84	10.72	11.20	11.03
Na_2O	1.55	1.81	1.57	1.40	1.53	1.64	2.54	2.53	2.10	1.66	1.75	1.78	1.95	1.84	1.57	1.69
K_2O	0.52	0.52	0.88	0.85	0.75	0.79	0.35	0.30	0.29	0.23	0.34	0.36	0.47	0.55	0.42	0.71
Cr_2O_3	0.05	0.00	0.07	0.04	0.02	0.00	0.00	0.00	0.05	0.13	0.02	0.04	0.00	0.00	0.00	0.00
NiO	0.00	0.00	0.00	0.00	0.00	0.15	0.04	0.04	0.00	0.00	0.00	0.00	0.09	0.08	0.00	0.02
F	0.00	0.08	0.00	0.00	0.09	0.12	0.00	0.00	0.00	0.00	0.00	0.00	0.00	0.00	0.00	0.08
Cl	0.05	0.05	0.08	0.05	0.00	0.00	0.00	0.00	0.03	0.03	0.07	0.08	0.00	0.00	0.01	0.00
Total	97.63	97.64	97.58	96.72	96.45	98.29	95.84	95.77	97.05	97.79	97.42	96.37	95.97	96.29	97.89	97.03
O=23**																
Si	6.274	6.214	6.265	6.324	6.364	6.330	6.136	6.254	6.180	6.174	6.188	6.300	6.121	6.110	6.391	6.264
Al_{tet}	2.808	2.769	2.623	2.541	2.478	2.417	2.697	2.447	2.947	2.910	2.951	2.790	3.014	2.900	2.924	2.865
Al^{vi}	1.726	1.786	1.735	1.676	1.636	1.670	1.864	1.746	1.820	1.826	1.812	1.700	1.879	1.890	1.609	1.736
Al^{iv}	1.082	0.983	0.888	0.865	0.842	0.747	0.833	0.701	1.127	1.084	1.139	1.090	1.135	1.010	1.315	1.129
Ti	0.092	0.063	0.107	0.121	0.102	0.113	0.082	0.087	0.068	0.061	0.037	0.094	0.038	0.074	0.046	0.085
Fe^{3+***}	0.249	0.416	0.262	0.206	0.297	0.427	0.665	0.726	0.413	0.490	0.371	0.247	0.335	0.411	0.141	0.231
Fe^{2+}	1.605	1.669	1.769	1.795	1.843	1.721	1.184	1.039	1.742	1.700	1.757	1.499	1.616	1.650	1.408	1.359
Mn	0.012	0.033	0.037	0.036	0.028	0.025	0.033	0.035	0.000	0.009	0.034	0.036	0.023	0.028	0.026	0.029
Mg	2.030	1.954	2.011	2.036	1.971	2.087	2.203	2.412	1.766	1.794	1.767	2.104	1.947	1.943	2.104	2.233
Ca	1.766	1.704	1.801	1.838	1.767	1.704	1.701	1.680	1.625	1.668	1.726	1.728	1.743	1.724	1.738	1.731
Na_{M4}	0.163	0.178	0.125	0.103	0.149	0.175	0.299	0.320	0.258	0.194	0.169	0.202	0.163	0.160	0.228	0.204
Na_A	0.278	0.340	0.328	0.304	0.298	0.294	0.435	0.408	0.346	0.281	0.334	0.309	0.405	0.375	0.212	0.276
K	0.097	0.098	0.167	0.163	0.144	0.151	0.067	0.057	0.055	0.043	0.064	0.068	0.090	0.105	0.077	0.133
Mg#****	0.558	0.539	0.532	0.531	0.517	0.548	0.650	0.699	0.503	0.513	0.501	0.584	0.546	0.541	0.599	0.622

* : FeO* was calculated as total iron

** : Cation was calculated based on 23-oxygens

*** : Fe^{3+} and Fe^{2+} were calculated based on Robinson et al. (1982)

**** : Mg#=Mg/(Mg+Fe^{2+}) in atomic

Table 4-7. Results from mineral thermobarometry in pyroxene granulites

CPX-PL-QTZ geothermobarometry

Sample No.		X_{An}	X_{Ab}	X_{CaTs}	X_{Si}	$LogK_{(1)}$	$LogK_{(2)}$	T	P
Chilas complex									
SM7	igneous								
	early	0.68	0.31	0.024	0.038	-1.56	-1.01	720	780
	peak	0.62	0.36	0.033	0.038	-1.33	-1.00	780	970
	later	0.74	0.25	0.049	0.029	-1.66	-1.10	690	630
NKA									
LT3	early	0.58	0.40	0.027	0.028	-1.50	-1.17	780	750
	peak	0.57	0.42	0.030	0.031	-1.39	-1.11	830	820
	later	0.66	0.33	0.019	0.022	-1.80	-1.26	640	480
LT8	early	0.68	0.32	0.026	0.024	-1.61	-1.19	740	630
	peak	0.56	0.43	0.031	0.036	-1.38	-1.05	830	890
	later	0.60	0.40	0.016	0.030	-1.82	-1.16	660	530
D8	early	0.51	0.47	0.023	0.036	-1.57	-1.09	740	750
	peak	0.49	0.48	0.059	0.030	-1.35	-1.05	850	950
	later	0.80	0.19	0.020	0.040	-1.73	-0.83	660	720
SKA									
PL4	igneous								
	early	0.62	0.38	0.022	0.033	-1.68	-1.11	710	690
	peak	0.68	0.31	0.033	0.042	-1.35	-0.94	780	1100
P8	igneous								
	early	0.54	0.45	0.025	0.033	-1.47	-1.12	790	770
	peak	0.55	0.44	0.034	0.040	-1.26	-1.00	870	1050
P5	early	0.57	0.42	0.026	0.039	-1.46	-1.03	750	830
	peak	0.59	0.41	0.030	0.051	-1.33	-0.91	760	960
PU5	early	0.52	0.46	0.030	0.049	-1.33	-0.95	760	950
	peak	0.56	0.43	0.038	0.047	-1.24	-0.93	810	1080

Temperature in °C, Pressure in MPa

Activities were calculated as $a_{CaTs} = 4 \cdot X_{Ca}^{M2} \cdot X_{Al}^{M1} \cdot X_{Al}^{T} \cdot X_{Si}^{T} \cdot \gamma_{CaTs}$, $a_{Ki} = X_{Ki} \gamma_{Ki}$.

$\log_{10} K_{(1)} = a_{CaTs}/a_{An}$, $\log_{10} K_{(2)} = a_{Si}/a_{An}$.

Table 4-8. Results from thermobarometry in pyroxene granulites and garnet granulites

		Grt-Cpx					Two Px	Grt-Cpx-Pl-Qtz				
Sample No.	Ref P†	T(K)	T(EG)	T(A)	T(PN)	T(G)	T(KR)	Ref T††	$P(M_{Fe})$	$P(M_{Mg})$	P(E)	P(PN)
Chilas complex												
SM7	600						1042					
NKA												
D8	1000	696	753	641	611	784		750	1123	922	871	830
1408	1000	776	822	721	699	842		800	1326	1021	939	902
SKA												
PL4	600						1183					
PL2	1000	778	812	722	782	806		800	1251	1142	1018	981
P8	600						1114					
P5	1000	796	831	736	808	836		800	1140	1105	961	923
Jijal complex												
PD2b	1200	758	790	679	642	781		750	1408	1193	1152	1111
LP1	1400	745	773	678	680	733		750	1568	1317	1228	1189
PD23	1400	930	938	853	783	883		850	1791	1633	1529	1496
PD25	1600	967	971	909	876	901		900	1998	1790	1610	1580

Temperature in °C, Pressure in MPa. Garnet-clinopyroxene geothermometer from T(K): Krogh (1988); T(EG): Ellis & Green (1979); T(A): Ai (1994); T(PN): Pattison & Newton (1988); T(G): Ganguly *et al.* (1996). Two pyroxene geothermometer from Kretz (1982). Garnet-clinopyroxene-plagioclase-quartz geobarometer from P(M): Moecher *et al.* (1988); P(E): Eckert *et al.* (1991) and P(PN): Perkins & Newton (1981). Fe and Mg gives the results for the Fe- and Mg-endmember reactions modeled by Moecher *et al.* (1988).

†Reference pressure to calculate temperature. ††Reference temperature to calculate pressure.

Table 4-9. Pressures estimated from the garnet-hornblende-plagioclase-quartz geobarometer of Kohn & Spear (1990) using estimated temperatures from the garnet-hornblende thermometer of Graham & Powell (1984).

Sample No.	X_{An}	Si_{Amp}	X_{Mg}	X_{Alm}	X_{Prp}	X_{Grs}	T(°C)	P(Mg)[1]	P(Fe)[1]
NKA									
BR6-1	0.60	6.23	0.70	0.514	0.280	0.185	626	700	710
BR6-2	0.56	6.43	0.66	0.491	0.302	0.188	703	720	730
BR6-3	0.58	6.43	0.64	0.493	0.304	0.186	725	700	710
1406	0.48	6.50	0.60	0.520	0.280	0.190	602	770	680
CH1-1	0.40	6.24	0.60	0.604	0.202	0.160	595	740	750
CH1-2	0.40	6.19	0.61	0.589	0.213	0.162	602	770	770
CH2"	0.40	6.25	0.69	0.562	0.252	0.136	550	690	700
CH4-1	0.31	6.32	0.58	0.619	0.180	0.145	566	760	760
CH4-2	0.34	6.23	0.56	0.620	0.191	0.139	598	760	760
SKA									
MA2*		6.06	0.57	0.605	0.164	0.196	607		
KY25	0.38	6.17	0.60	0.563	0.185	0.213	635	900	910
1509	0.35	6.19	0.53	0.550	0.200	0.190	712	930	900
PA3-1	0.35	6.37	0.62	0.520	0.202	0.226	743	990	970
PA3-2	0.33	6.29	0.62	0.547	0.182	0.218	624	940	950
PU4	0.38	6.21	0.52	0.553	0.064	0.214	698	920	920

*: plagioclase-free assemblage

[1]: P(Mg) and P(Fe) represent the pressures estimated from the calibrations of Mg- and Fe-endmember reactions, respectively.

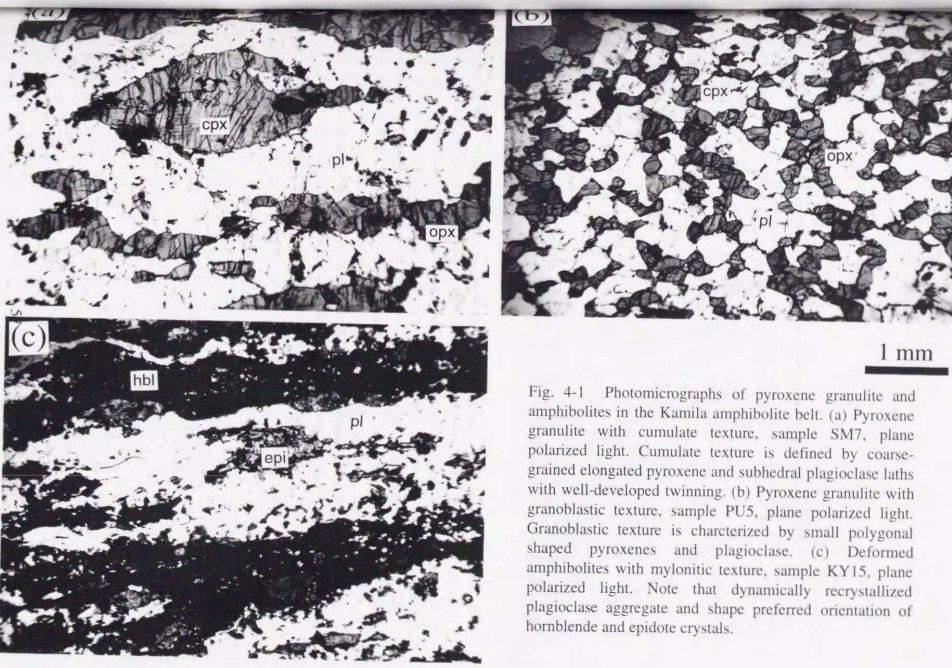

Fig. 4-1 Photomicrographs of pyroxene granulite and amphibolites in the Kamila amphibolite belt. (a) Pyroxene granulite with cumulate texture, sample SM7, plane polarized light. Cumulate texture is defined by coarse-grained elongated pyroxene and subhedral plagioclase laths with well-developed twinning. (b) Pyroxene granulite with granoblastic texture, sample PU5, plane polarized light. Granoblastic texture is charcterized by small polygonal shaped pyroxenes and plagioclase. (c) Deformed amphibolites with mylonitic texture, sample KY15, plane polarized light. Note that dynamically recrystallized plagioclase aggregate and shape preferred orientation of hornblende and epidote crystals.

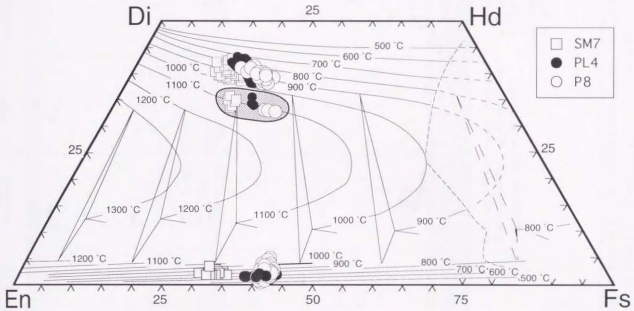

Fig. 4-3. Pyroxene quardrilateral showing trend of pyroxenes with cumulate texture from the pyroxene granulites in the Kohistan arc. Chemical composition of clinopyroxene in pyroxene quardrilateral is almost augite and that of orthopyroxene is hyperthene. Orthopyroxene has calcic core, whereas igneous clinopyroxene is characterized by calcic-poor at core. SM7 is a pyroxene granulite from the Chilas complex. PL4 and P8 are the relict pyroxene granulites from the SKA. Polythermal contours of 100 °C intervals at 500 MPa from Lindsley (1983). Shaded area represents reconstructed chemical composition of core of clinopyroxene involving exsolution lamellae of orthopyroxene. The highest temperature is over 1100 °C and it suggests the crystallization temperature of clinopyroxene from the gabbroic magma. The minimum temperature is concentrated around 800 °C and it suggests the re-equilibrium temperature under granulite facies metamorphism.

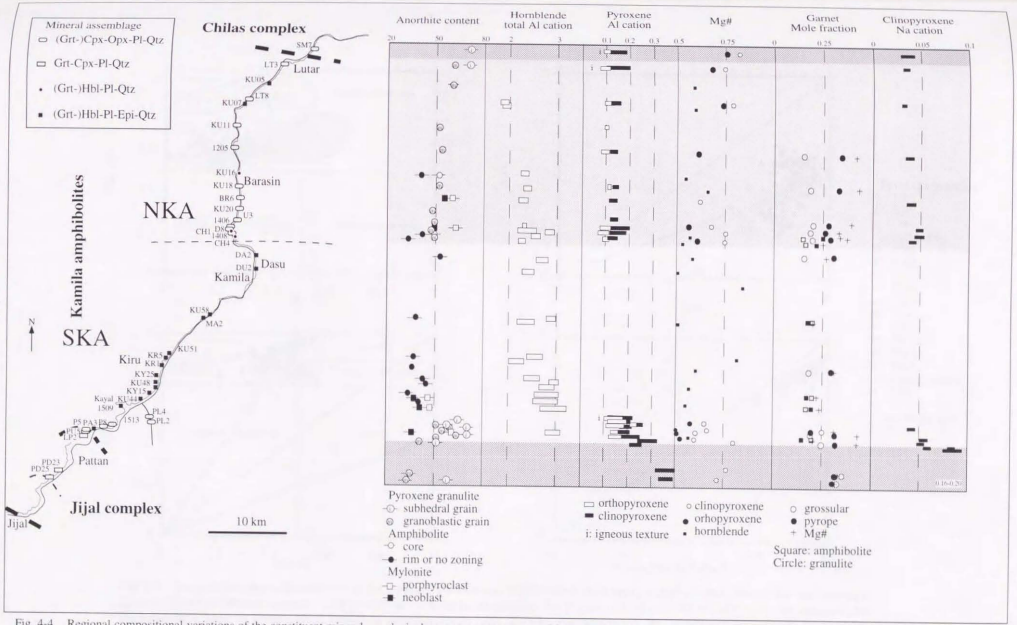

Fig. 4-4. Regional compositional variations of the constituent minerals as plagioclase, pyroxenes, garnet and hornblende in the southern Kohistan complex along the Indus Valley. The An content of plagioclase is generally decreasing toward the south. Al total cation of hornblende is continuously increasing southward. Al cation in pyroxenes is also increasing toward the south. The Al cation in igneous clinopyroxene range widely in comparison to metamorphic pyroxene. Mg# (Mg/(Mg+Fe)) in pyroxenes from the relict pyroxene granulites decrease toward the south throughout the KAB, whereas Mg# in clinopyroxene from the garnet granulite in the Jijal complex are relatively higher value. Grossular content in garnet slightly increases southward. Na cation in clinopyroxene increases toward the south.

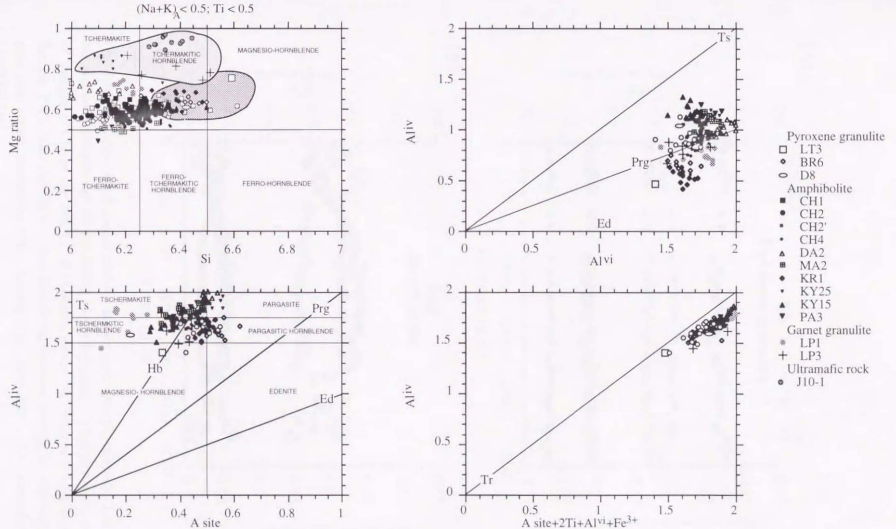

Fig. 4-5. Compositional plots of hornblendes in the pyroxene granulite and amphibolite in the Kamila amphibolite belt. Sample No. and lithologic types are shown in different symbols. (a) Mg numbers vs. Si for hornblendes on the diagram of Leake (1978). (b) Al^{IV} vs. A-site occupancy for the hornblende. Most of hornblende is plotted on exchange vector (Hb). Ts: tchermak substituton, Hb: hornblende substitution, Pg: pargasite substituion, Ed: edenite substitution. (c) Al^{IV}vs. $Al^{VI}$for hornblende. Most of hornblende is plotted on exchange vector of pargasite substitutuion. (d) A site+2Ti+Al^{VI}+Fe^{3+} vs. $Al^{IV}$for hornblende. $Al^{IV}$is sytematically lower than Al^{VI}. Tr: tremolite substitution.

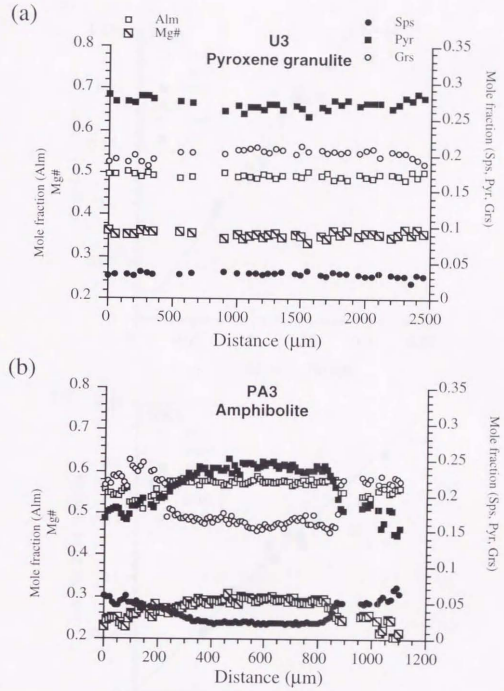

Fig. 4-6. Compositional zoning profiles across garnet porphyroblasts. Locality of the analyzed samples are shown in Fig. 4-4. (a) Garnet within pyroxene granulite of Sample U3 from the NKA. (b) Garnet within the deformed amphibolites of Sample PA3 from the SKA. Note that discontinuous zoning, in especially X_{Grs}, near rim. Alm, almandine; Pyr, pyrope; Sps, spessartine; Grs, grossular; Mg#, Mg/(Mg+Fe).

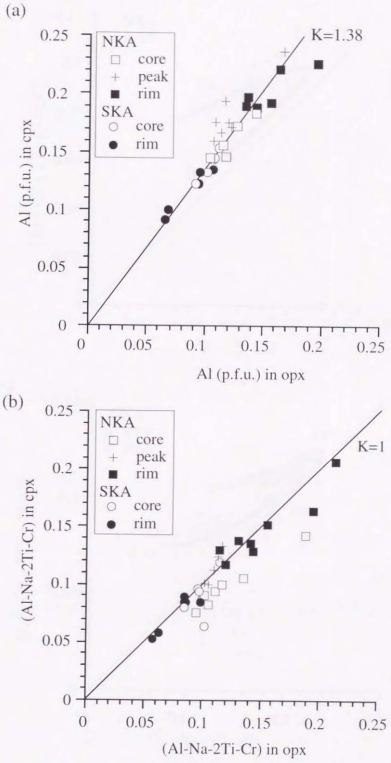

Fig. 4-7. Distribution Al and tschermak components between orthopyroxene and clinopyroxene in pyroxene granulites in the Kamila amphibolite belt. (a) Total Al cation in orthopyroxene vs. total Al cation in clinopyroxene. (b) Comparison of tschermak components between orthopyroxene and clinopyroxene assuming alliron is divalent cation. Slope represents a partition coefficient between two pyroxenes.

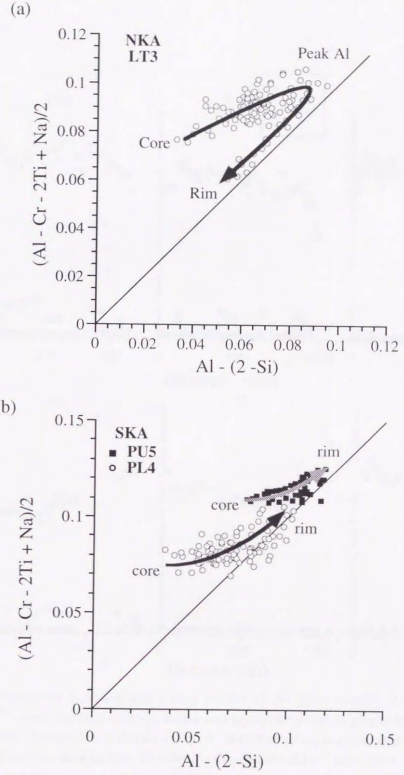

Fig. 4-8. (Al+Na-2Ti-Cr)/2 versus Al-(2-Si) for a single clinopyroxene grain with cumulate texture of the NKA (a) and SKA (b). The values of (Al+Na-2Ti-Cr)/2 are systematically higher than those of Al-(2-Si) and the difference is large at core. Thick arrows indicate change of composition corresponding to the zoning from core to rim.

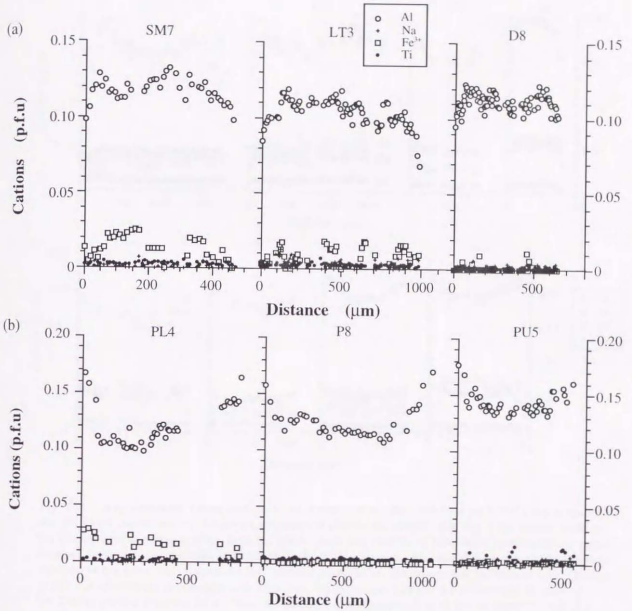

Fig. 4-9. Representative compositional zoning profiles of Al (open circles), Na (+), Ti (solid circles) and Fe^{3+} (open squares) contents across orthopyroxene grains in plagioclase matrix from pyroxene granulite. Sample No. is shown in Fig. 5. Note that orthopyroxene involves vanishingly small Na and Ti contents in any cases. In most of case, calculated Fe^{3+} value show wide variations from the NKA and SKA. (a) Al zoning profiles in orthopyroxene from the NKA. Al content slightly increase toward rim and then suddenly decrease at the rim. (b) Al zoning profiles in orthopyroxene from the SKA. Al content simply increase toward the rim.

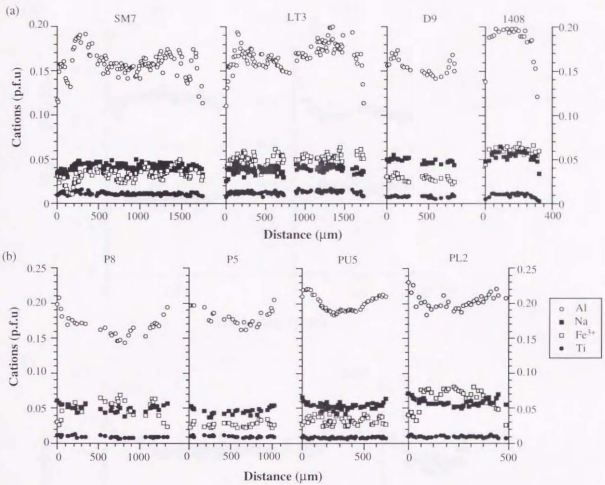

Fig. 4-10. Representative zoning profiles of Al- (open circles), Na- (solid squares), Fe^{3+} - (open squares) and Ti- (solid circles) across clinopyroxene grains in plagioclase matrix. See Fig. 5 for sample locations. (a) Compositional zoning profiles from the NKA. Note that profiles of Al-content showing flat or slight increase from core to inner rim and sudden decrease at outer rim. Na- and Ti-contents tend to slightly decrease at the outer rim. Calculated Fe^{3+} -content scattered variable range and oscillate at core. Zoning profiles of Al-contents in clinopyroxene with granoblastic texture (Sample 1408) showing decrease at rim. (b) Zoning profiles from the SKA. Note that profiles of Al-content showing flat or slight increase at core and increase toward the outermost margin near rim. Ti-contents tend to slightly decrease at outer rim. Zoning of calculated Fe^{3+}-content with scattered value is oscillate at core and abruptly decrease at rim. Al- and Na-contents of clinopyroxene with granoblastic texture (Sample PU5) shows increase toward the rim.

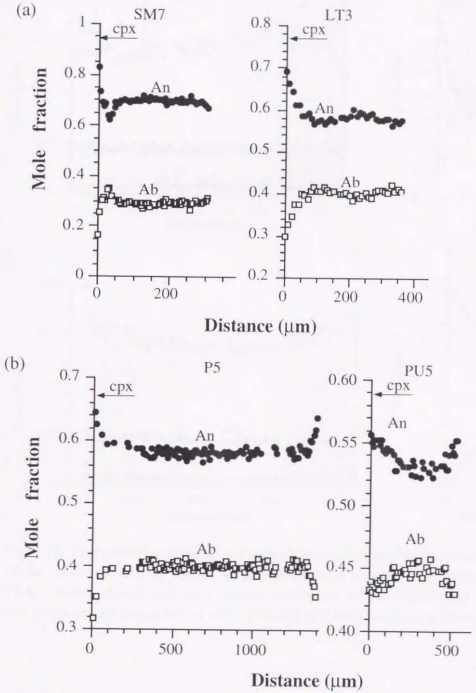

Fig. 4-11. Representative zoning profiles of anorthite (An) and albite (Ab) components in plagioclase in contact with clinopyroxene. The zoning profile at rim of plagioclase and clinopyroxene is different by neighboring minerals. (a) Zoning profiles in plagioclase from the NKA. An-contents in plagioclase once decrease and then abruptly increase toward the neighboring clinopyroxene grain. (b) Zoning profiles in plagioclase from the SKA. An-contents in plagioclase simply increase toward the rim.

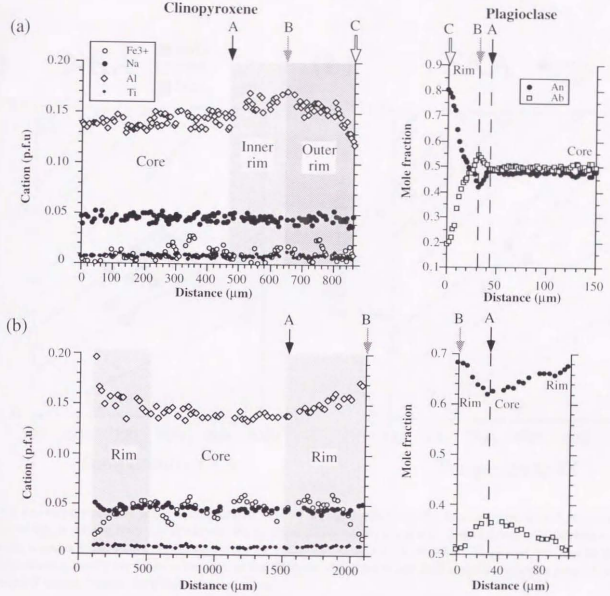

Fig. 4-12. Representative relations of compositional zoning profiles across the touching pairs of plagioclase and clinopyroxene. (a) Sample D8 from the NKA. (b) Sample PL4 from the SKA. Solid, shaded and open arrows correspond to the equilibrium points between clinopyroxene and plagioclase of early, peak and later metamorphic conditions, respectively.

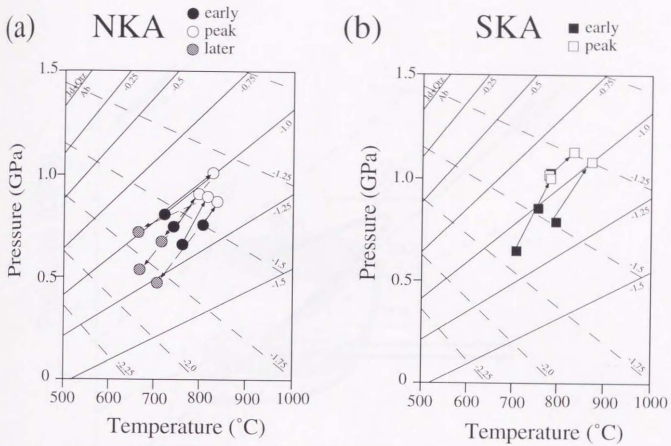

Fig. 4-13. Pressure-temperature projections estimated from Al-zoning thermobarometry in clinopyroxene and plagioclase. Isopleths of $\log_{10}K$ derived from Anovitz (1991) for reactions albite = jadeite + quartz (dashed lines), and anorthite = Ca tschermaks + quartz (solid lines). (a) Results from the NKA. (b) Results from the SKA. In general, the highest peak conditions increase toward the south in the both of the NKA and SKA. Solid and dashed arrows indicates prograde and retrograde *P-T* vectors from the each samples, respectively.

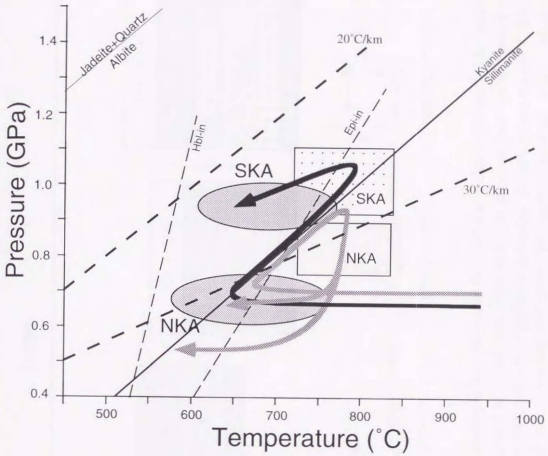

Fig. 4-14. Shaded squares represent approximate *P-T* stability field from pyroxene granulites based on garnet-clinopyroxene-plagioclase-quartz barometry. Dark stippled areas show *P-T* stability field from amphibolites on the basis of garnet-hornblende geothermometry (Graham & Powell, 1984) and garnet-hornblende-plagioclase-quartz geobarometer (Kohn & Spear, 1991). Early stage of the whole *P-T* trajectories is based on the trajectories deduced from Al zoning thermobarometry (Anovitz, 1991). Retrograde paths of *P-T* trajectories combined with the *P-T* conditions from pyroxene granulites and amphibolites based on the garnet-bearing geothermobarometry. The overall *P-T* paths from the NKA and the SKA represent the CW-ITD-IBC and ACW-IBC ones, respectively.

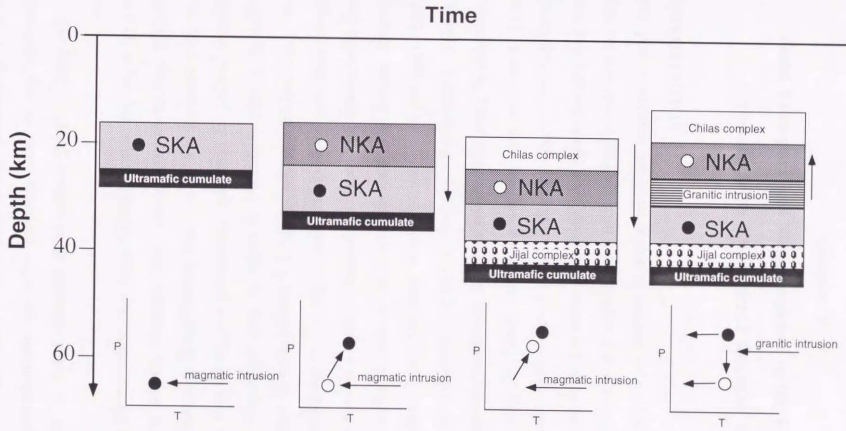

Fig. 4-15. Schematic model of magmatic underplating process in the Kohistan paleo-island arc. The higher pressure part of the Kohistan arc is composed of initial thin crust and then pressure increase is caused by substantial gabbroic intrusion at middle crustal depth. After gabbroic intrusion, garnitic sheets width of 10 km intruded between the NKA and SKA and took place the isothermal decompression of the NKA. Finally, gabbroic mass cooled at the same depth accompanied with regional hydration (amphibolitization).